

WP3

Monitoring network improvement for coastal flooding and extreme weather risk management

Activity 3.2

Radar monitoring network for coastal flooding and extreme weather

D3.2.2 Radar based valuable products for extreme weather events monitoring



PROJECT AND ACTIVITY DETAILS

Project Acronym	AdriaMORE
Project title	Adriatic DSS exploitation for MONitoring and Risk management of coastal Extreme weather and flooding
Funding Line	Priority Axis 2, Specific Objective 2.2
Project Partners	LP Abruzzo Region (Italy) P1 Dubrovnik and Neretva Region (Croatia) P2 Meteorological and hydrological service (Croatia) P3 National Research Council (Italy)
Starting date	January 1, 2018
Activity number	3.2
Activity Title	Radar monitoring network for coastal flooding and extreme weather
Work Package	WP3: Monitoring network improvement for coastal flooding and extreme weather risk management
Activity Summary	Activity 3.2, within Work Package 3, is devoted to improve the effectiveness of radars measurements by mean the creation of radar composite by utilizing data provided by Italian and Croatian radar network
Deliverable number	3.2.2
Deliverable Summary	This deliverable is aimed at describing the useful radar products to be used against extreme weather events, it can be applied at radars having different technical characteristics
Main Author	Errico Picciotti, errico.picciotti@aquila.infn.it
Main Author's organization	CETEMPS
Other Author's	Saverio Di Fabio and Stefano Barbieri
Data of issue	November 30, 2018
Total Number of pages	46
Distribution list	Italy-Croatia CBC Programme, AdriaMORE partners

This document has been produced with the contribution of the EU co-financing and the Interreg Italy-Croatia CBC Programme. The content reflects the author's views; the Programme authorities are not liable for any use that may be made of the information contained therein.

Table of contents

1. Introduction	Pag. 4
2. Ramp chain to process volumetric radar data	Pag. 6
2.1 First-step correction	Pag. 8
2.2 Partial beam blocking correction	Pag. 11
2.3 Path attenuation correction	Pag. 14
2.4 Total quality characterisation	Pag. 16
2.4.1 Radar system technical parameters	Pag. 18
2.4.2 Non-meteorological echo	Pag. 19
2.4.3 Partial beam blocking	Pag. 19
2.4.4 Long range measurement	Pag. 21
2.4.5 Rain path attenuation	Pag. 23
2.4.6 Inhomogeneous vertical profile of reflectivity	Pag. 25
2.5 Examples of application	Pag. 27
3. Radar products for extreme weather monitoring	Pag. 29
3.1 Maximum of reflectivity	Pag. 30
3.2 Convective storm detection	Pag. 32
3.3 Nowcasting	Pag. 35
3.4 Precipitation estimation	Pag. 37
3.5 Vertically Integrated Liquid	Pag. 40
3.6 Hail detection	Pag. 42
4. References	Pag. 44

1. INTRODUCTION

Hydro-meteorological hazards like convective outbreaks leading to torrential rain and floods are among the most critical environmental issues in Adriatic area.

The inherent spatial and temporal variability of precipitation makes rainfall one of the most difficult geophysical variables to measure anywhere, and yet it is one of the most important for advancing hydro-meteorological predictions. In particular, improving local flood and flash flood forecasting as well as other extreme weather events requires accurate quantitative rainfall information at small temporal (minutes) and spatial (hundreds of meters) scales.

Arguably, weather radar's capability to monitor precipitation at high spatial and temporal scales has stimulated great interest and support within the hydro-meteorological community. Increasingly, radar-based products are necessary for efficient civil protection, transport safety, ecology, agriculture and water management.

AdriaMORE project goal is to improve an existing integrated hydro-meteorological risk management platform focusing on the Adriatic coastal areas of Italy and Croatia.

To this end, one of AdriaMORE's specific objective is the improving the **effectiveness of radar measurements** in Adriatic coastal area by means of the creation of a rain composite utilizing data provided by Italian and Croatian radar network. This objective has been performed in the action 3.2 of the WP3 of AdriaMORE project whose the main result is constituted by the **Output entitled "One radar network mosaic data SW to enhance the monitoring coastal flood"**.

Two deliverables have contributed to the achievement of the above project Output:

- one aimed at describing the radar's mosaic algorithm chain developed and the related composite products (**deliverable 3.2.1**)
- one aimed at describing the useful radar products to be used against extreme weather events, it can be applied at radars having different technical characteristics (**deliverable 3.2.2**).

The first deliverable is described in another document while the **deliverable 3.2.2**, subject of this paper is aimed at describing the useful radar products to be used against extreme weather events, it can be applied at radars having different technical characteristics (single or dual polarization, S-, C- and X-band). These products, applicable at single radar level, can be used together or in place of the composite products generated by the radar mosaic system called CRAMS (Cetemps Radar Advanced Mosaic Software) described in deliverable 3.2.1 and sketch in **figure 1** where the modules devoted at generate single radar products, described in this report, are highlighted.

Given the heterogeneity of the radar input data and having to create products suitable for every type of system all products will be generated from the volume corrected reflectivity data. However, the number of errors burdening radar data is very high and it is practically impossible to eliminate all the errors satisfactorily [**Villarini, 2010**] on the other hand, precise information about the data reliability is important for the end user. Thus, before the products generation, once a raw volume scan is fully received, the data must be processed through the specific processing chain called RAMP to eliminating, compensating or at least to identifying the most common error sources for each device. RAMP description is given in the **chapter 2** whereas the products can be generated at single radar level are described in the **chapter 3**. All references cited are reported in the **chapter 4**.

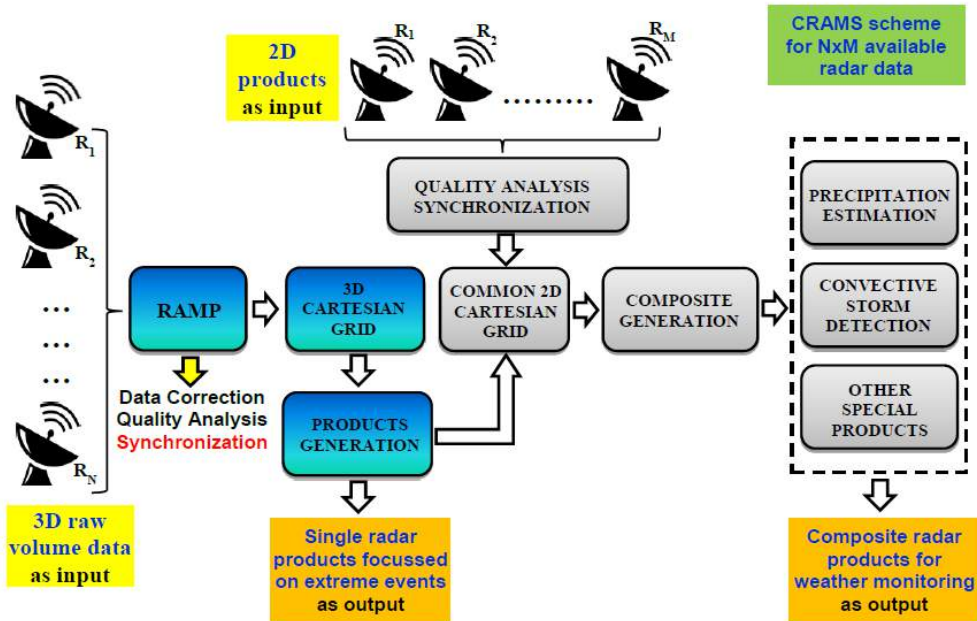


Figure 1 The flowchart of the radar mosaic system (CRAMS) developed within AdriaMORE project, the modules objective of this report are highlighted

Examples of application are given for the radar systems already described in the deliverable 3.2.1, anyway for the reader convenience their location and some technical characteristics are resumed in figure 2.



RADAR	BAND	PEAK POWER	MAX RANGE
M. MIDIA	C	250 kW	240 Km
TORTORETO	X	25 kW	120 Km
CEPAGATTI	X	10 kW	108 Km
CINGOLI	X	25 kW	120 Km
L'AQUILA	X	25 kW	60 Km
BILOGORA	S	550 kW	240 Km
PUNTIJARKA	S	550 kW	240 Km
OSIJEK	S	550 kW	240 Km

Figure 2 The location (left panel) and some technical characteristics (right panel) of the radars whose data are utilized in this report

2. RAMP CHAIN TO PROCESS VOLUMETRIC RADAR DATA

There are numerous sources of errors that affect radar measurements of reflectivity volumes or surface precipitation, which have been comprehensively discussed by many authors [e.g. Collier, 1996; Meischner, 2004; Šálek, 2004; Michelson, 2005]. Hardware sources of errors are related to electronics stability, antenna accuracy, and signal processing accuracy [Gekat, 2004]. Other non-meteorological errors are results of electromagnetic interference with the sun and other microwave emitters, attenuation due to a wet or snow (ice) covered radome, ground clutter [Germann, 2004], anomalous propagation of radar beam due to specific atmosphere temperature or moisture gradient [Bebbington, 2007], and biological echoes from birds, insects, etc. Next group of errors is associated with scan strategy, radar beam geometry and interpolation between sampling points, as well as the broadening of the beam width with increasing distance from the radar site.

Moreover, the beam may be blocked due to topography [Bech, 2003] and by nearby objects like trees and buildings, or not fully filled when the size of precipitation echo is relatively small or the precipitation is at low altitude in relation to the antenna elevation (so called overshooting).

Apart from the above-mentioned non-precipitation errors, meteorologically related factors influence precipitation estimation from weather radar measurements. Attenuation by hydrometeors, which depends on precipitation phase (rain, snow, melting snow, graupel or hail), intensity, and radar wavelength, particularly C and X band, may cause the strong underestimation in precipitation, especially in case of hail. Another source of error is Z–R relation which expresses the dependence of precipitation intensity R on radar reflectivity Z. This empirical formula is influenced by drop size distribution, which varies for different precipitation phases, intensities, and types of precipitation: convective or non-convective [Šálek, 2004]. The melting layer located at the altitude where ice melts to rain additionally introduces uncertainty into precipitation estimation. Since water is much more conductive than ice, a thin layer of water covering melting snowflakes causes strong overestimation in radar reflectivity. This effect is known as the bright band [Battan, 1973; Goltz, 2006]. Moreover, the non-uniform vertical profile of precipitation leads to problems with the estimation of surface precipitation from radar measurement [e.g. Franco, 2002; Germann, 2004; Einfalt, 2008], and these vertical profiles may strongly vary in space and time [Zawadzki, 2006].

Dual-polarization radars have the potential to provide additional information to overcome many of the uncertainties in contrast to situation when only the conventional reflectivity Z and Doppler information is available [Illingworth, 2004].

Characterization of the radar data quality is then necessary to describe uncertainty in the data taking into account potential errors that can be quantified as well as the ones that can be estimated only qualitatively. Generally, the following quality metrics are used as more suitable:

- total error level, i.e. measured value \pm standard deviation expressed as measured physical quantity (radar reflectivity in dBZ, precipitation in mm h⁻¹, etc.),
- quality flag taking discrete value, in the simplest form 0 or 1 that means “bad” or “excellent” data,
- quality index as unitless quantity related to the data errors, which is expressed by numbers e.g. from 0 to 1.

A sketch of the main source of uncertainty is given in **figure 3**.

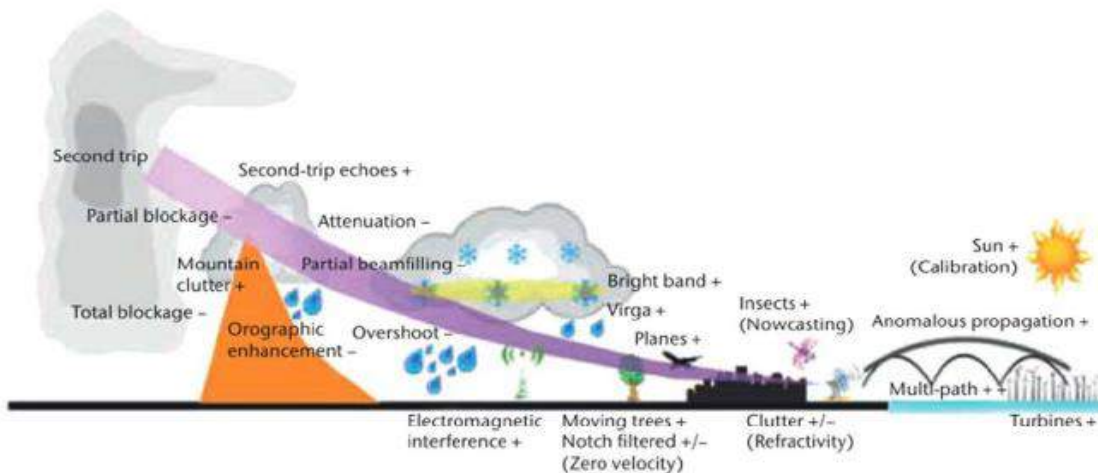


Figure 3 The weather radar can detect many things besides weather targets, this schematic illustrates many of these features. The + or – signs indicate whether the radar reflectivity is augmented or diminished by these features. These artefacts need to be removed for quantitative applications

To address the sources of errors, in the framework of AdriaMORE project, a specific processing chain called **RAMP (Radar Advanced Multiband Processing)** has been developed starting from some results of ADRIARadNet and CapRadNet projects.

After a radar scan, raw data are generated as so-called volumes, i.e. 3-D polar data and once a raw volume scan is fully received, the data are processed through the RAMP in order to compensating or at least to identifying the most common error sources for each radar device. That to ensure harmonized technical and software platforms on which each radar data, with different features, can be processed before the products generation at single radar level as well as before the composite.

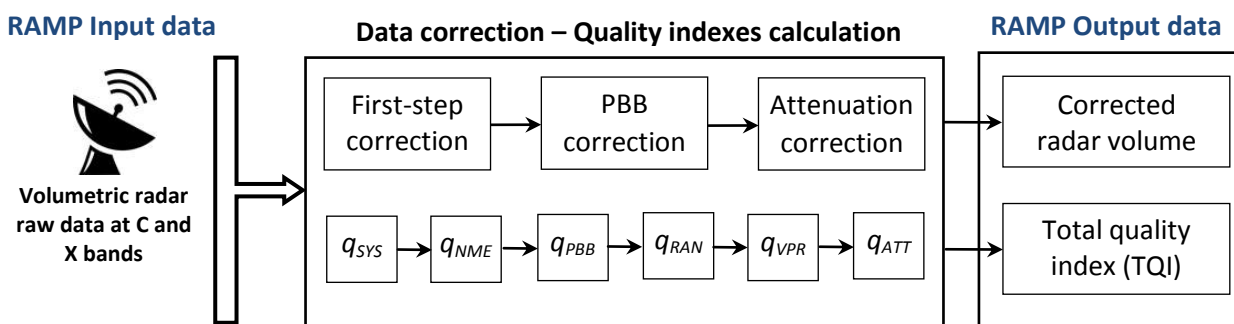


Figure 4 Weather radar data processing chain (RAMP)

The scheme of RAMP chain is presented in **figure 4**. The employed algorithms are functionally divided into two paths: one for data corrections and the second for data quality characterization. Particular quality algorithms can be switched on or off in the scheme. In general, algorithms for the 3D data quality control and characterization can be divided into categories based on analysis of: scan geometry, reflectivity data structure and technical characteristics.

The scheme should be an objective procedure, i.e. independent of platform (quality of data from different radar could be easy to compare) for the application at different radar data.

The main steps of data correction and quality characterization within the proposed RAMP chain are described in the next paragraphs.

2.1 First-step correction

For each radar, a specific first-step correction of volumetric data is applied. Residual ground-clutter, specks, WLAN interference, biological and others non-meteorological echoes have been removed from the reflectivity Z field mainly by exploiting the textural spatial correlation of meteorological targets with respect to artifacts [Barbieri, 2017]. Uncertain data are flagged but not removed.

The spatial pattern of the precipitation field is considered as the most essential criterion while developing algorithms for removal of such spurious echoes.

The texture of radar signatures is also used to verify the spatial self-consistency. The texture function (Tex) is a spatial root mean square function, defined over a box of $N \times N$ contiguous pixels as:

$$Tex_N(X) = \sqrt{\frac{1}{N^2} \sum_{n=-N/2, \neq 0}^{N/2} \sum_{m=-N/2, \neq 0}^{N/2} [x(n) - x(0)]^2} \quad (1)$$

where x is a generic radar observable (Z in such case) and $x(0)$ is the box center. The Tex function is also used as a clutter removal tool since a mask is introduced as follows:

$$Tex_N(x) \leq t_{threshold}(x) \quad (2)$$

where $t_{threshold}$ is an ad hoc threshold defined to identify the meteorological target with respect to environmental and artificial clutter, to be tuned on both radars system and environmental features.

Four examples of application of reflectivity correction are shown in figures 5-8 for the Monte Midia, Cepagatti, Bilogora and Osijek radar.

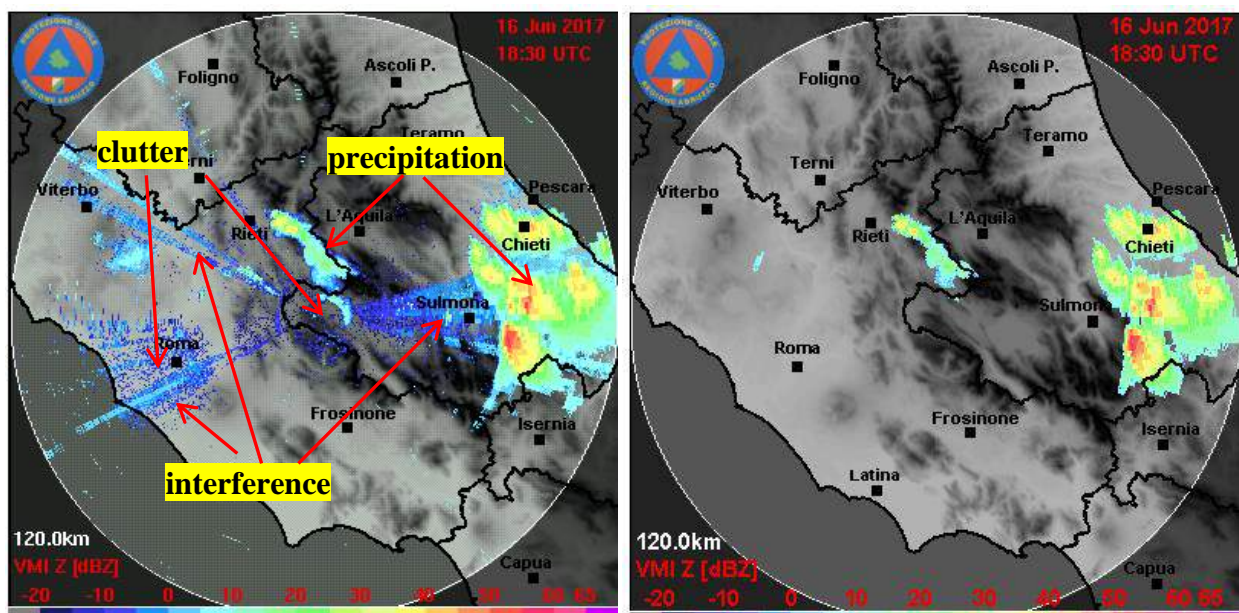


Figure 5 Uncorrected reflectivity image (left panel) as input at RAMP chain and the related output (right panel) after that “First step correction” has been applied at Monte Midia radar for the precipitation event occurred on June 16, 2017

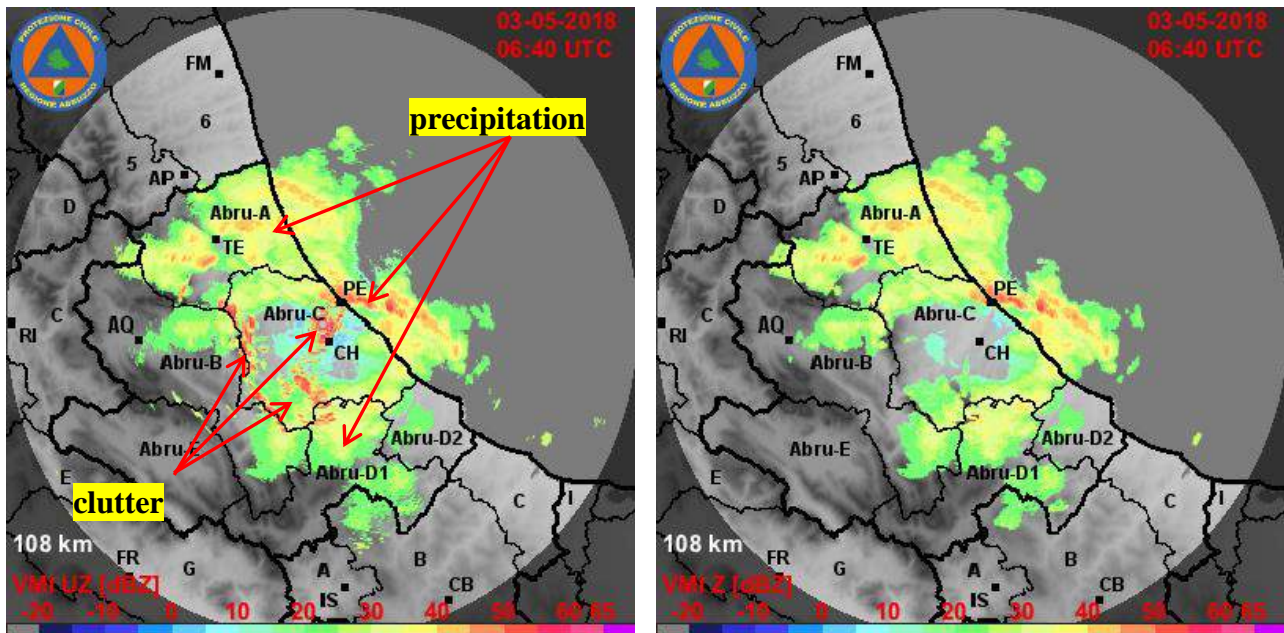


Figure 6 Uncorrected reflectivity image (left panel) as input at RAMP chain and the related output (right panel) after that “First step correction” has been applied for Cepagatti radar for the precipitation event occurred on June 16, 2017

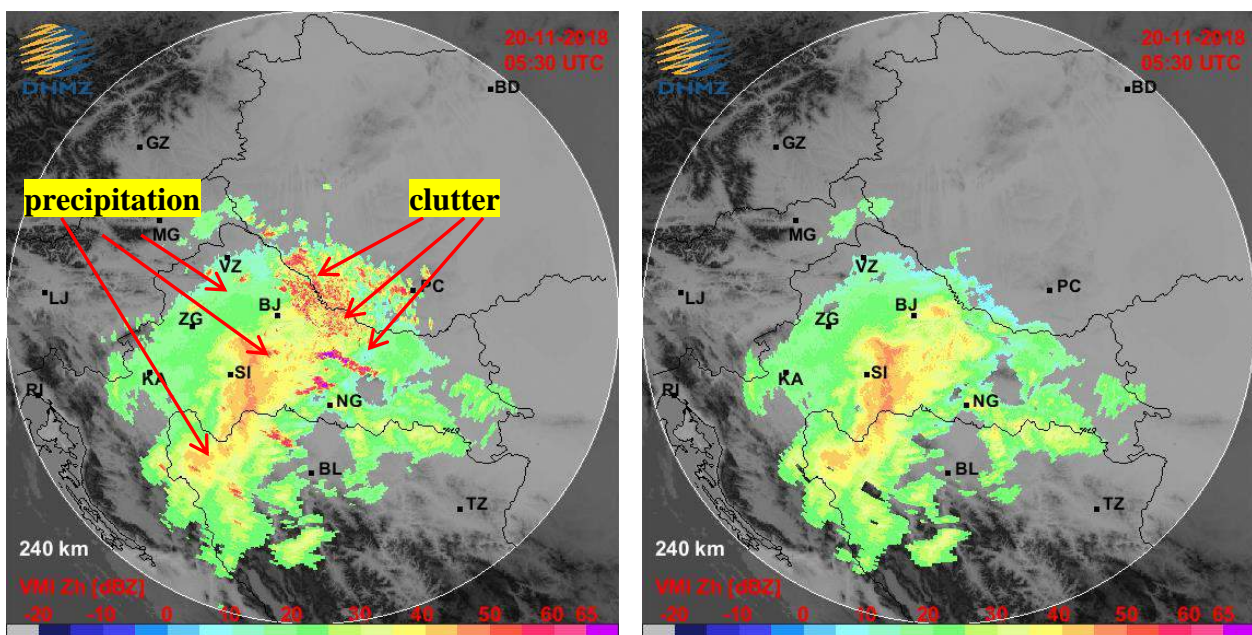


Figure 7 Uncorrected reflectivity image (left panel) as input at RAMP chain and the related output (right panel) after that “First step correction” has been applied for Bilogora radar for the precipitation event occurred on November 20, 2018

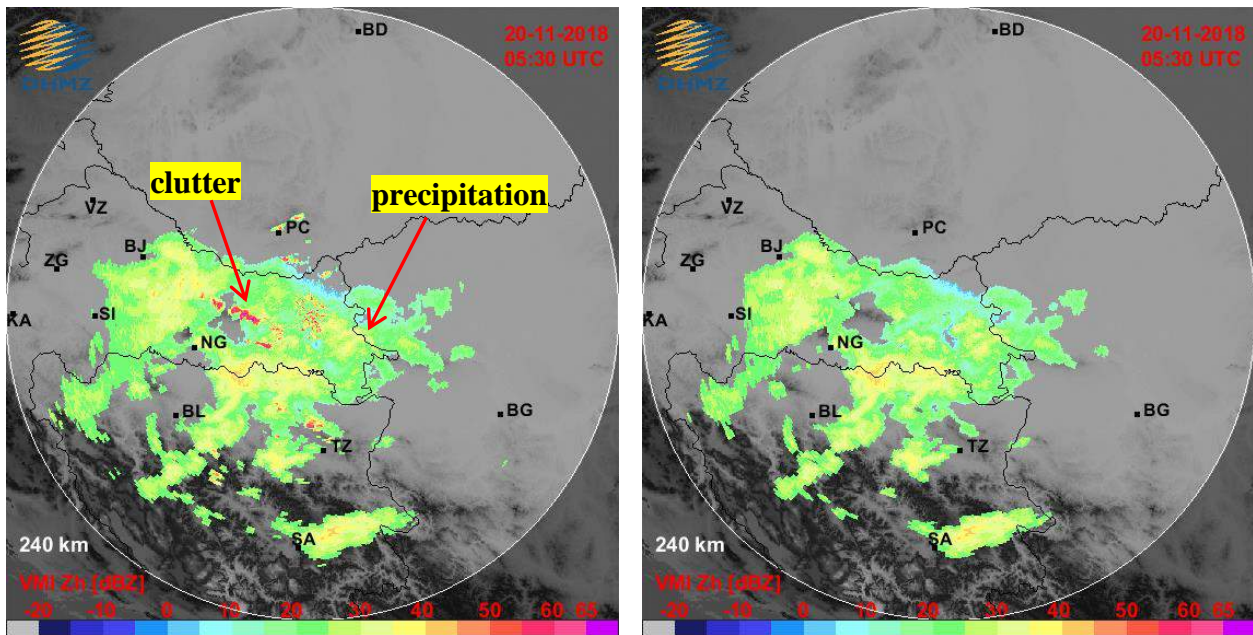


Figure 8 Uncorrected reflectivity image (left panel) as input at RAMP chain and the related output (right panel) after that "First step correction" has been applied for Osijek radar for the precipitation event occurred on November 20, 2018

For dual-polarization systems, in addition, a median smoothing filter and bias correction is applied to the differential reflectivity (Z_{dr}), a compensation is applied to the correlation coefficient (ρ_{hv}) and the differential phase (Φ_{dp}) has been processed by a multistage smoothing filter for Kdp estimation [Barbieri, 2014]. An example of application of Z_{dr} correction is shown in **figure 9** for Cingoli radar.

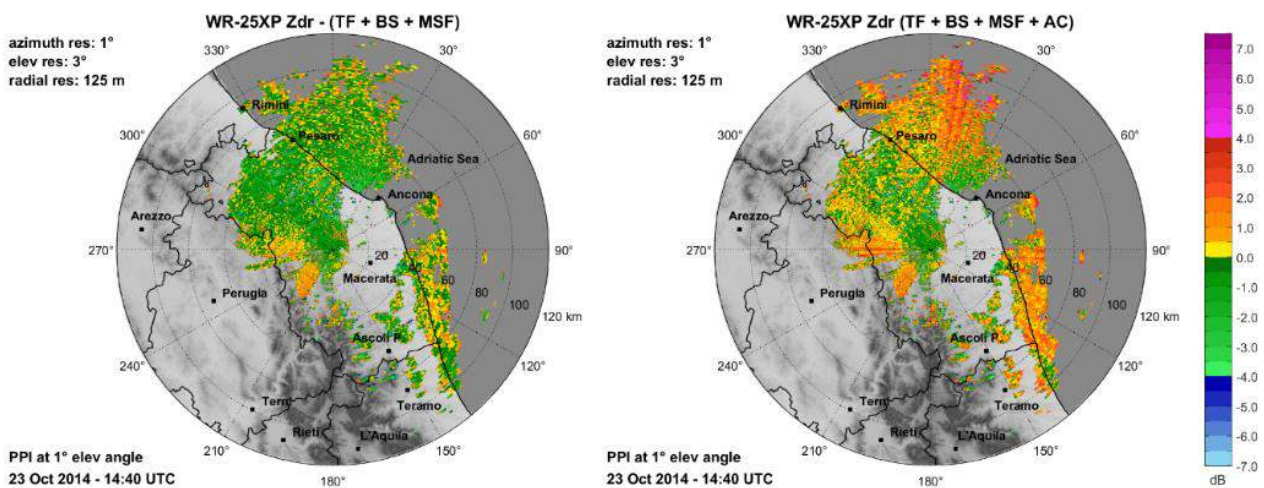


Figure 9 Measured Z_{dr} (left panel) and that corrected for attenuation (right panel) applied at Cingoli radar during a rainy event

2.2 Partial beam blockage correction

Radars operating in complex orographic areas usually suffer from partial or total beam blockage by surrounding targets at their lowest elevation scans. The need for radar quantitative precipitation estimates in such environments led to the development of PBB (Partial Beam Blockage) corrections. For this product a correction scheme based on [Bech, 2003] method has been developed and here briefly illustrated.

When a radar beam intercepts a mountain, two situations are possible: 1) only part of the beam cross section illuminates the intercepted topography (partial blockage), or 2) the radar beam is completely blocked (total blockage).

A geometrical approach is applied to calculate the degree of the beam blockage. This approach is based on calculation of which part of radar beam cross-section is blocked, for any elevation angle, by any topographical object. For this purpose the degree of PBB is computed from a high-resolution (250 m) digital terrain map (DTM), the radar technical characteristics and its sampling strategy.

The percentage area of the radar beam cross section blocked by topography may be expressed as a function of the radius of the beam cross section a and the difference y between the average height of the terrain H_{dem} and the center of the radar beam h (see figure 10). Depending on the relative position of the beam height respect to topography, y may be either positive or negative.

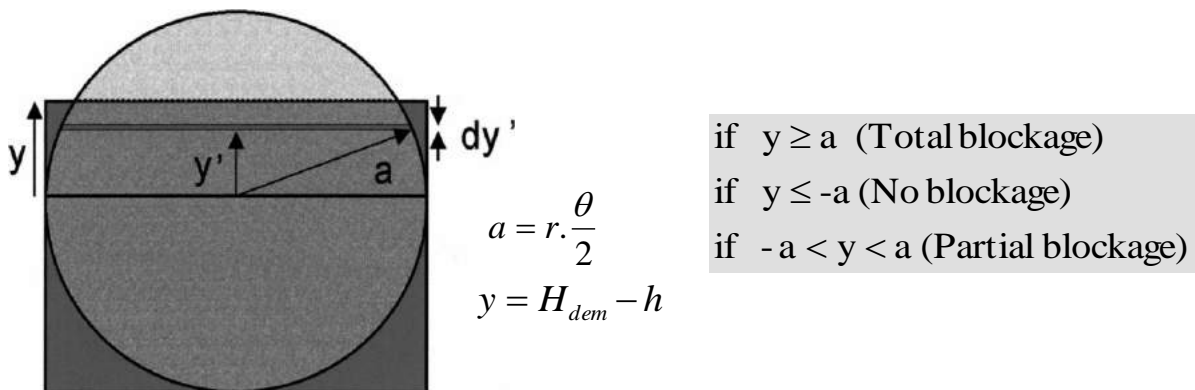


Figure 10 Elements considered in the radar beam blockage function: a is the radius of the radar beam cross section, y the difference between the center of the radar beam and the topography, dy' the differential part of blocked beam section, and y' the distance from the center to dy'

According to these definitions, partial beam blockage occurs when $-a < y < a$, total beam blockage means that $y \geq a$ and, finally, $y \leq -a$ implies there is no blockage at all. Using the notation introduced above, it can be seen that PBB may be written as

$$PBB = \frac{y\sqrt{a^2 - y^2} + a^2 \arcsin \frac{y}{a} + \frac{\pi a^2}{2}}{\pi a^2}$$

On the other hand, the height of the center of the radar beam h is given at a distance r by the expression [Doviak, 1993]:

$$h = y\sqrt{r^2 + (k_e R)^2} + 2k_e R \sin \theta - k_e R + H_0$$

where R is the earth's radius, k_e is the ratio between R and the equivalent earth's radius, θ is the antenna elevation angle, and H_0 is the antenna height.

Information about atmospheric propagation conditions is contained in k_e , which may be written in terms of the refractivity gradient (VRG) as:

$$k_e = \frac{1}{1 + R \left(\frac{dN}{dH} \right)}$$

The usual value for k_e in the first kilometer of the troposphere, assuming the normal VRG of -40 km^{-1} , is approximately $4/3$.

For each radar pixel (or bin) of the entire volume scan PBB is computed and usually is expressed in percentage. The Partial Beam Blockage correction can be applied to radar bins partially shielded according to vary schemes [Tabary, 2007; Fulton, 1998; Fornasiero, 2005].

In the scheme here adopted the beam of less than 10% is considered negligible and is not corrected, vice versa if the PBB exceed 70% the radar pixel is rejected (the pixel is marked as "no data"). If radar bin is partially shielded between 10% and 70% will be modified the radar equivalent reflectivity factor measurements by adding a correction factor (CF) varying between 1–4 dB and depending on the degree of occultation (**table 1**).

<i>Occultation (%)</i>	<i>CF (dB)</i>
0 – 10,	0
11 – 29	+1
30 – 43	+2
44 – 55	+3
56 – 63	+4
63 – 70	+5
> 70	rejected

Table 1 Partial occultation corrections factor (CF)

The corrected reflectivity (Z_c) is computed from the measured one (Z) by mean:

$$Z_c = Z + CF$$

where both reflectivities are expressed in dBZ.

As an example, in **figure 11** are shown the visibility maps at the first operational elevation for the radars of Bilogora, Osijek and Puntijarka. In the same figure the visibility map of Monte Midia, Cepagatti and Cingoli radars at given elevation angles is also shown.

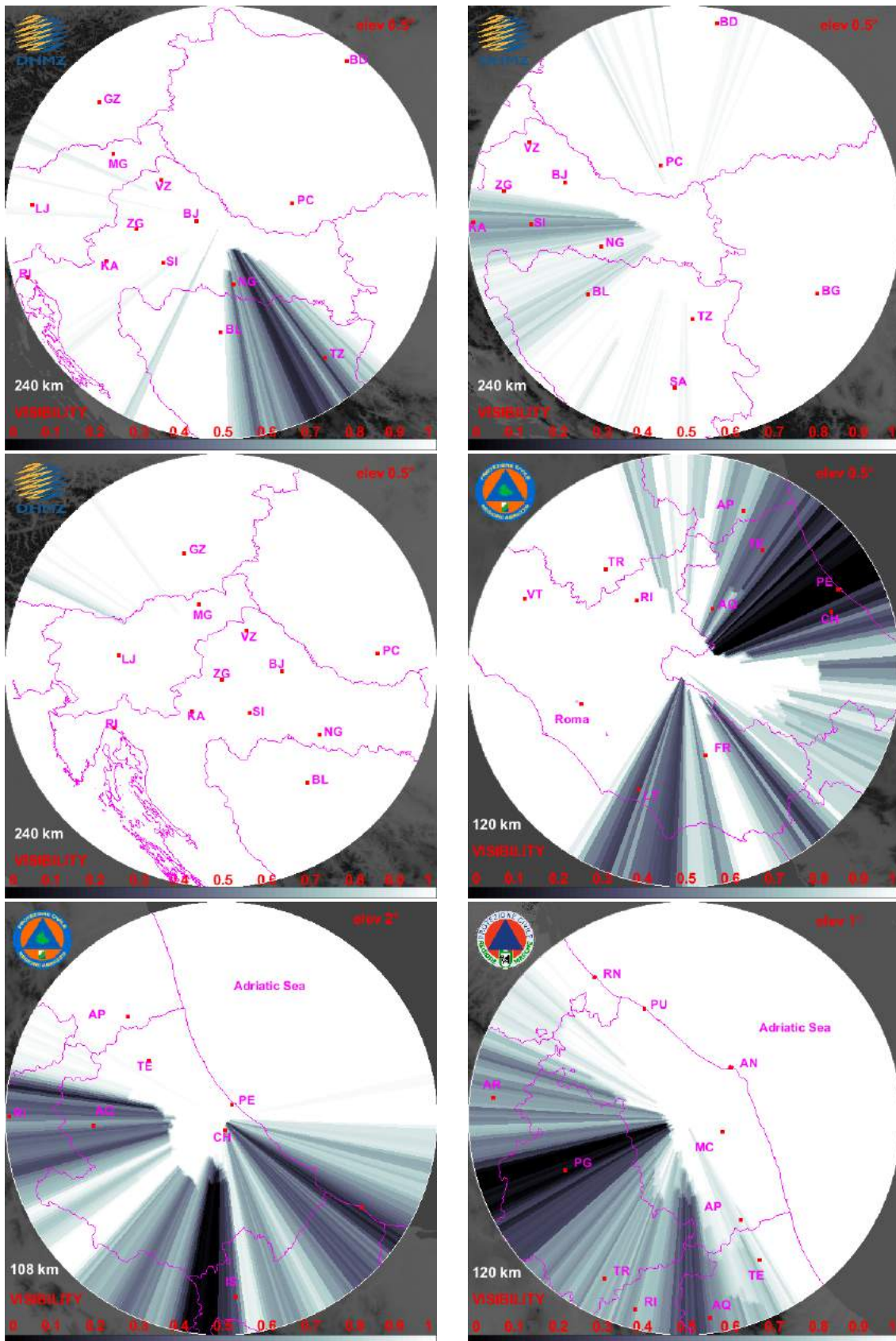


Figure 11 Visibility maps (black, no visibility and white, full visibility) for the radars of Bilogora (top left), Osijek (top right), Puntijarka (central left), Monte Midia (central right), Cepagatti (bottom left) and Cingoli (bottom right) at given elevation angles

2.3 Path attenuation correction

The attenuation that the radar signal undergoes in the presence of heavy precipitation determines an underestimation of the measured reflectivity and differential reflectivity that increases with the increase in the distance from the radar and the intensity of the precipitation in progress. This problem is particularly important in the X-band and can also lead to the complete extinction of the signal [Maki, 2012]. We must therefore try to compensate both the reflectivity (Z) and the differential reflectivity (Z_{dr}), the latter present in the double polarization systems only.

The attenuation correction algorithms, for polarimetric radar, are applied at Z and Z_{dr} (corrected by the first step correction module) using the reconstructed differential phase Φ_{dp} [Bringi, 2001]. The differences of the reconstructed phase, between a cell and the other in distance, are connected to the attenuation increments along the path through the coefficients α and β :

$$\begin{aligned} Z_c &= Z + \alpha [\Phi_{dp}(r_N) - \Phi_{dp}(r_0)] = Z + PIA \\ Z_{drc} &= Z_{dr} + \beta [\Phi_{dp}(r_N) - \Phi_{dp}(r_0)] = Z_{dr} + PIA \end{aligned}$$

In the two equation $\alpha = 0.28$, $\beta = 0.04$ for the X band [Tabary, 2008] while $\alpha = 0.08$, $\beta = 0.03$ for the C band [Gourley, 2007] r_N and r_0 are, respectively, the farthest cell and the initial cell along the path of the beam signal radar.

The terms Z_c and Z_{drc} indicate the correct quantities while the PIA is the integrated path attenuation that undergoes the radar signal in the presence of precipitation between r_0 and r_N considering the return path too.

For single-polarization systems, the PIA is instead calculated using an iterative procedure that uses only the measurement of Z . The attenuation coefficient (k , in dB/km) and the reflectivity (Z , in $\text{mm}^6 \text{m}^{-3}$) are typically correlated by a power law $k = aZ^b$ with a and b appropriate coefficients depending by radar band. The bidirectional attenuation between two adjacent bins ($A_{(i-1,i)}$), expressed in dB, can be calculated using the above relationship, where L is the radial resolution of the bin (in km) and Z_i is the incorrect (i.e. measured) reflectivity in the i -th bin.

$$A_{(i-1,i)} = 2Lk = 2L\alpha Z_i^b$$

Through the multiplicative factor 2, we take into account both the “forward path” of the electromagnetic and the “return” in the direction of the radar. Therefore, an iterative procedure is used which involves the estimation of the integrated bidirectional attenuation (PIA) along the whole beam path. The PIA, integrated by the position of the radar (first bin) to the bin $i-1$, can be obtained according to the formula:

$$PIA_{(0,i-1)} = \sum_{j=1}^{i-1} A_{(j-1,j)}$$

Starting from the measured reflectivity Z_i the correct reflectivity $Z_{C(i)}$ in the bin i -th can be calculated according to the following relation:

$$Z_{C(i)}|_{dB} = Z_i|_{dB} + PIA_{(0,i-1)} + A_{(i-1,i)}$$

Obviously, this method can be applied at dual polarization system too, if the differential phase has no good quality or in operational context being computationally less expensive.

Find in **figure 12** three examples of correction for the attenuation at different radar frequencies (X-, C- and S- bands).

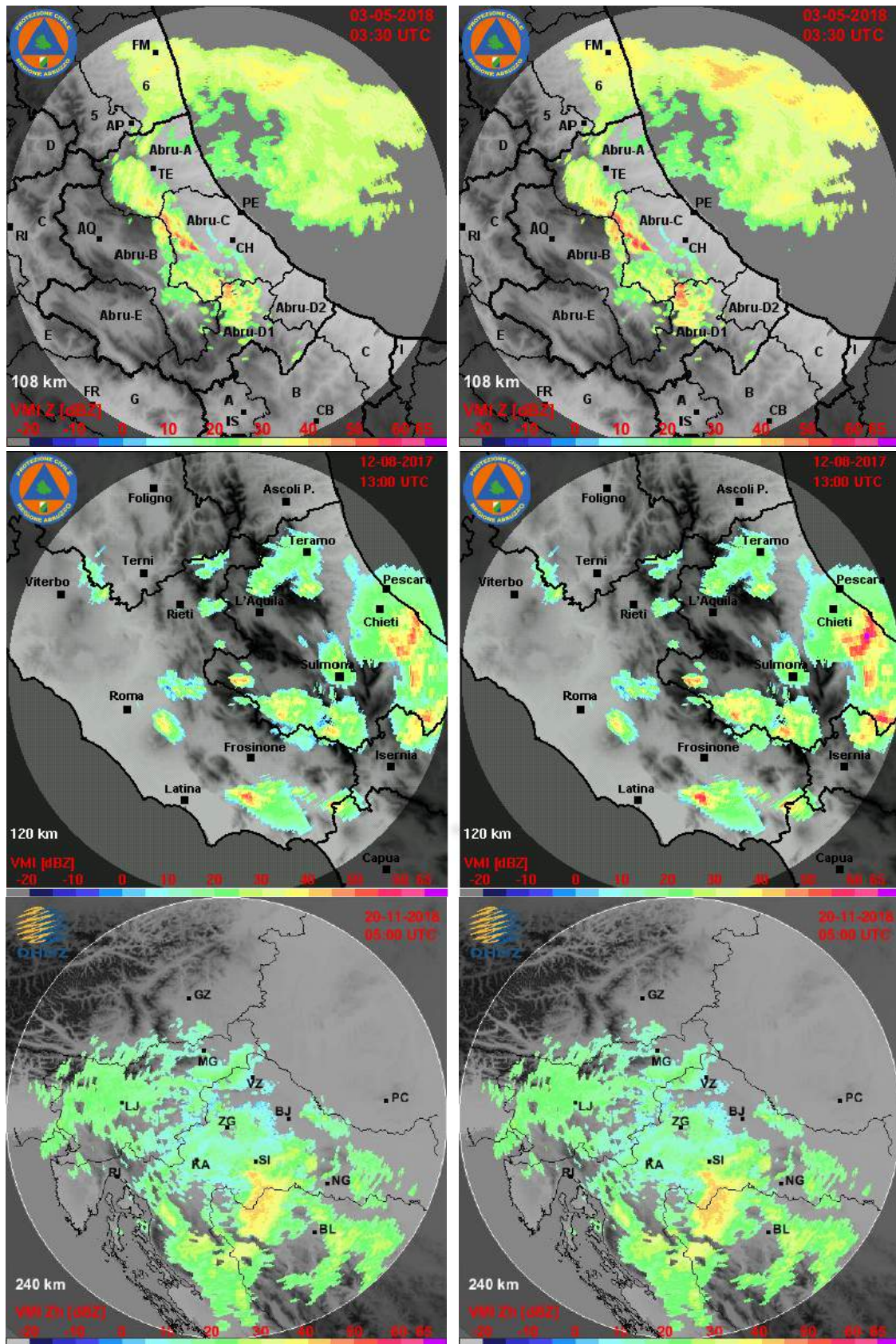


Figure 12 VMI map of uncorrected reflectivity (left) and corrected for the attenuation (right) using the iterative method for a X- C- and S-band weather radar located at Cepagatti (first row), M. Midia (second row) and Puntijarka (third row)

2.4 Total quality characterization

The quantitative estimation of error magnitude is necessary not only in order to gain general knowledge about data uncertainty but also to apply quality information in further data processing, e.g. in the generation of standard or user-related specific products. One of the most common approaches in the characterisation of the quality of weather radar data is to employ (q_i), which is defined as a unitless quantity that provides information on the data reliability in a digital scale.

The idea of the quality index scheme is based on selection of quality factors, determination of their quality indices and computation of one total quality index.

Assuming that any radar systems are well maintained, the quality analysis, for AdriaMORE purpose, has been focused on the following error sources: radar technical parameters q_{SYS} , non-meteorological echoes q_{NME} , beam blocking q_{PBB} , distance from the radar q_{RAN} , rain attenuation q_{ATT} and height of measurement q_{VPR} . All these quality indexes are resumed in the **table 2** and discussed in the following in separate sections which comprise a description of the algorithm for data quality characterization and some examples of application.

For each error an individual quality index (q_i) is calculated in each radar pixel volume through appropriate tests, giving as output an unitless quantity expressed by numbers from 0 (bad quality) to 1 (excellent quality).

If one of the input variables, after data quality procedure, results to not satisfy a predefined quality standard, it is flagged as no quality data and thus discarded or corrected.

Quality Index	Source of error	Note
q_{SYS}	Radar system technical parameters	It is static within the whole radar range as well as in time and taken into account several factors as in [Osrodka, 2012]
q_{NME}	Non-meteorological echo	Pixel affected by non-meteorological echoes are removed, for the uncertain pixel a value of 0.5 is applied, the others data are set to 1.
q_{PBB}	Partial beam blocking	It is computed from the corrected data taking into account the PBB value as in [Barbieri, 2017]
q_{RAN}	Long range measurement	This quality factor decreases with increasing distance from the radar, it is computed as in [Rinollo, 2013]
q_{ATT}	Rain path attenuation	It is computed from the corrected data taking into account the PIA value as in [Barbieri, 2017]
q_{VPR}	Inhomogeneous vertical profile of reflectivity	The compensation of this effect is not performed in RAMP, the quality index associated is estimated as in [Friedrich,2006]

Table 2 Group of quality index and related source of errors to which they refer

Computation of the total quality index (TQI) is the final step in estimation of radar volume data quality. In each radar pixel, the total quality index, which is treated as an overall quality information, is determined from a combination of all quality indices applying one of the formulae such as minimum value, additive or multiplicative operator. The last seems to be the most appropriate for the present aim due to its open form:

$$TQI = q_{SYS} \cdot q_{NME} \cdot q_{PBB} \cdot q_{RAN} \cdot q_{ATT} \cdot q_{VPR}$$

It can be noticed that the total quality index TQI equals zero if at least one of the individual quality indices q_i equals zero when such a formula is used, some examples of TQI are given in **figure 13**.

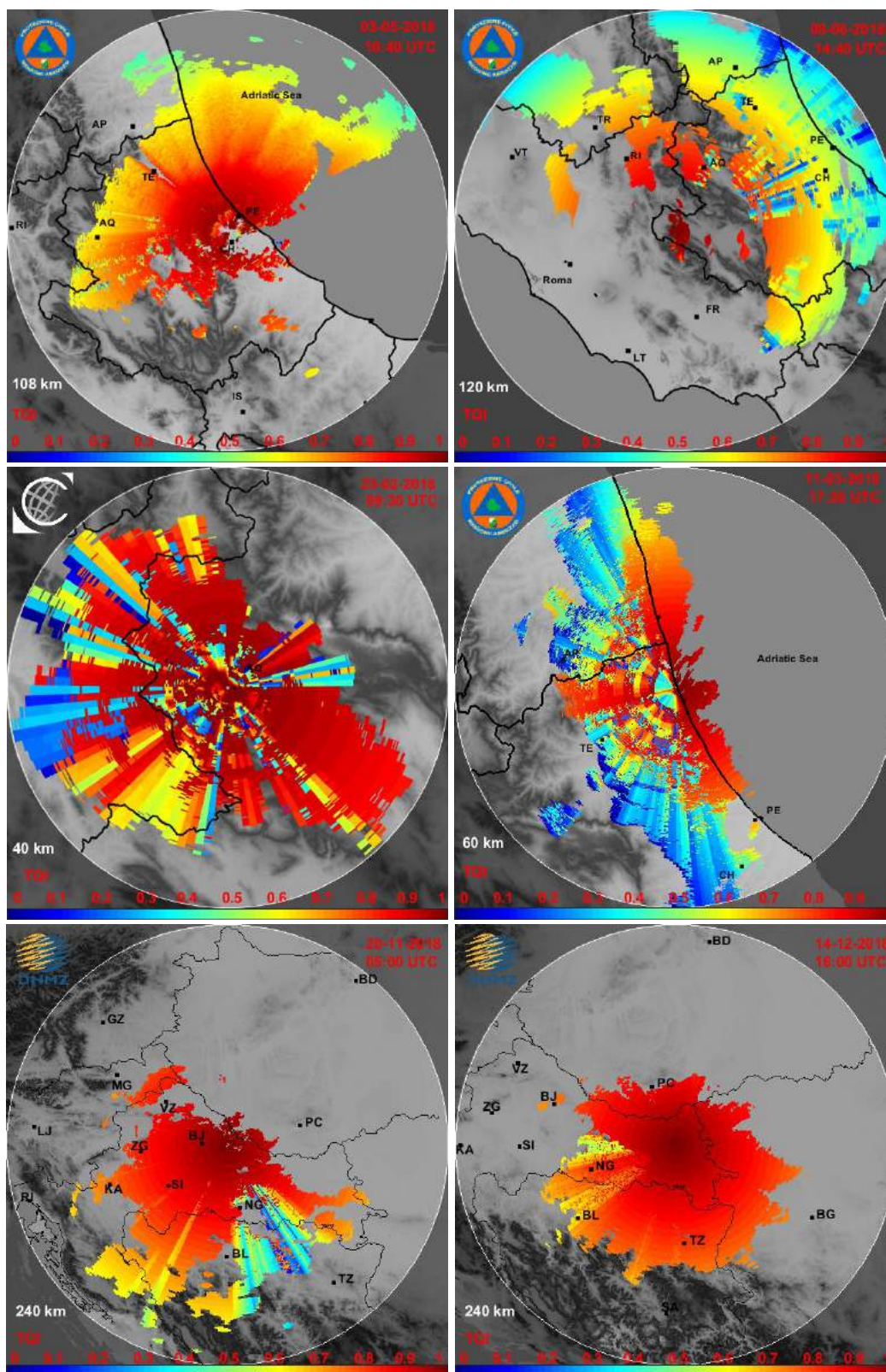


Figure 13 Examples of the TQI images for Cepagatti (top left), Monte Midia (top right), L'Aquila (central left), Tortoreto (central right), Bilogora (bottom left) and Osijek (bottom right) radars

2.4.1 Radar system technical parameters

The quality factor q_{SYS} aims to provide a quality taking into account a set of technical radar parameters that can impact on data quality.

A set of such factors, listed in **Table 3**, is based on EUMETNET OPERA Programme findings [Holleman, 2006; Osrodka, 2012]. It has complemented with other parameters.

All the quality factors are static within the whole radar range as well as in time (apart from the date of last electronic calibration). The threshold values for which any factor become lower than 1 have been set according to the authors' experience.

Technical parameters taken into account in q_{SYS} calculation	Symbol and threshold values
Operating frequency affects attenuation in precipitation	$q_{band} = \begin{cases} 1 & C \text{ or } S \text{ band} \\ 0.9 & X \text{ band} \end{cases}$
Beam width affects area of measurement averaging	$q_{bw} = \begin{cases} 1 & \text{beamwidth} \leq 1^\circ \\ 0.9 & \text{beamwidth} > 1^\circ \end{cases}$
Minimal detectable signal affects sensitivity to snow and drizzle detection	$q_{mds} = \begin{cases} 1 & MDS \leq -110 \text{ dBm} \\ 0.9 & MDS > -110 \text{ dBm} \end{cases}$
Antenna Speed affects measurement precision	$q_{as} = \begin{cases} 1 & \text{antenna speed} \leq 15^\circ/\text{sec} \\ 0.9 & \text{antenna speed} > 15^\circ/\text{sec} \end{cases}$
Radome attenuation causes measurement overestimation	$q_{rad} = \begin{cases} 1 & \text{radome attenuation is corrected} \\ 0.9 & \text{radome attenuation is NOT corrected} \end{cases}$
Date of last electronic calibration affects measurement precision	$q_{cal} = \begin{cases} 1 & \text{Date of last electronic calibration} \leq 180 \text{ days} \\ 0.9 & \text{Date of last electronic calibration} > 180 \text{ days} \end{cases}$
Height of the radar site affects measurement precision	$q_{hei} = \begin{cases} 1 & \text{radar site} \leq 1000 \text{ m} \\ 0.9 & \text{radar site} > 1000 \text{ m} \end{cases}$

Table 3 Quality factors related to the main radar system technical parameters

All the factors affect individual quality index, q_{SYS} connected with radar system parameters according to formula:

$$q_{SYS} = q_{band} \cdot q_{bw} \cdot q_{mds} \cdot q_{as} \cdot q_{rad} \cdot q_{cal} \cdot q_{hei}$$

It is assumed that lack of one set of information from **table 3** still allows generation of the q_{SYS} value, but the individual factors connected with the missing information is set as equal to 0.9.

If more than three quality factors are missing then the total q_{SYS} is treated as 'no data' (as a consequence the total quality index of the analysed data is also set as TQI = 'no data').

2.4.2 Non-meteorological echo

The ground-clutter can be removed at a level of radar system software and/or in post-processing utilizing customized algorithms. It is worth mentioning that usually the correction of radar images due to contamination by ground clutter is commonly made at a level of radar system software which uses statistical or doppler filtering but the portion of signal not removed, called residual clutter, will remain as part of many of the products if not removed in the post-processing.

Apart from ground clutter, other phenomena such as specks, external interference signals (e.g. from the sun and Wi-Fi emitters), biometeors (flocks of birds, swarms of insects), anomalous propagation echoes (so called anaprop) and sea clutter, are considered as non-meteorological clutter. Because various types of non-precipitation echoes can be found in radar observations, in practice individual sub-algorithms must be developed in post-processing to address each of them.

Pixel affected by non-meteorological echoes are removed in the “first step correction”, for the uncertain pixel a value of 0.5 is applied, the others data are set to 1.

$$q_{NME} = \begin{cases} 0 & \text{for non - meteorological pixel} \\ 0,5 & \text{for uncertain pixel} \\ 1 & \text{for meteorological pixel} \end{cases}$$

Even if rejected in the first module of the RAMP, we have symbolically assigned a zero quality to the pixel marked as non-meteorological echoes.

2.4.3 Partial beam blocking

A quality of measurement burdened by beam blockage dramatically decreases. The quality index q_{BB} of the pixel where the radar beam is considered as blocked can be expressed by the formula:

$$q_{PBB} = \begin{cases} 1 & \text{for } PBB \leq 0.1 \\ 0.9 & \text{for } 0.1 \leq PIA \leq a_{PBB} \\ 1 - PBB & \text{for } PIA > a_{PBB} \end{cases}$$

where the maximum quality has been assigned to the pixel non-corrected and the coefficient a_{PBB} has been set as 0.7 being the PBB compensated up to 0.7 ([Bech, 2007; Tabary, 2007]).

Even if rejected in the second module of the RAMP, we have symbolically assigned a $(1-PBB)$ quality to the pixel with PBB greater than 0.7 given that, the quality associated with the beam blocking, without compensation, can be set as the complementary of the PBB.

Figure 14 show some examples of the partial beam blocking quality index for VMI products of various radar. In each pixel q_{BB} is computed from the elevation which contributes to the VMI.

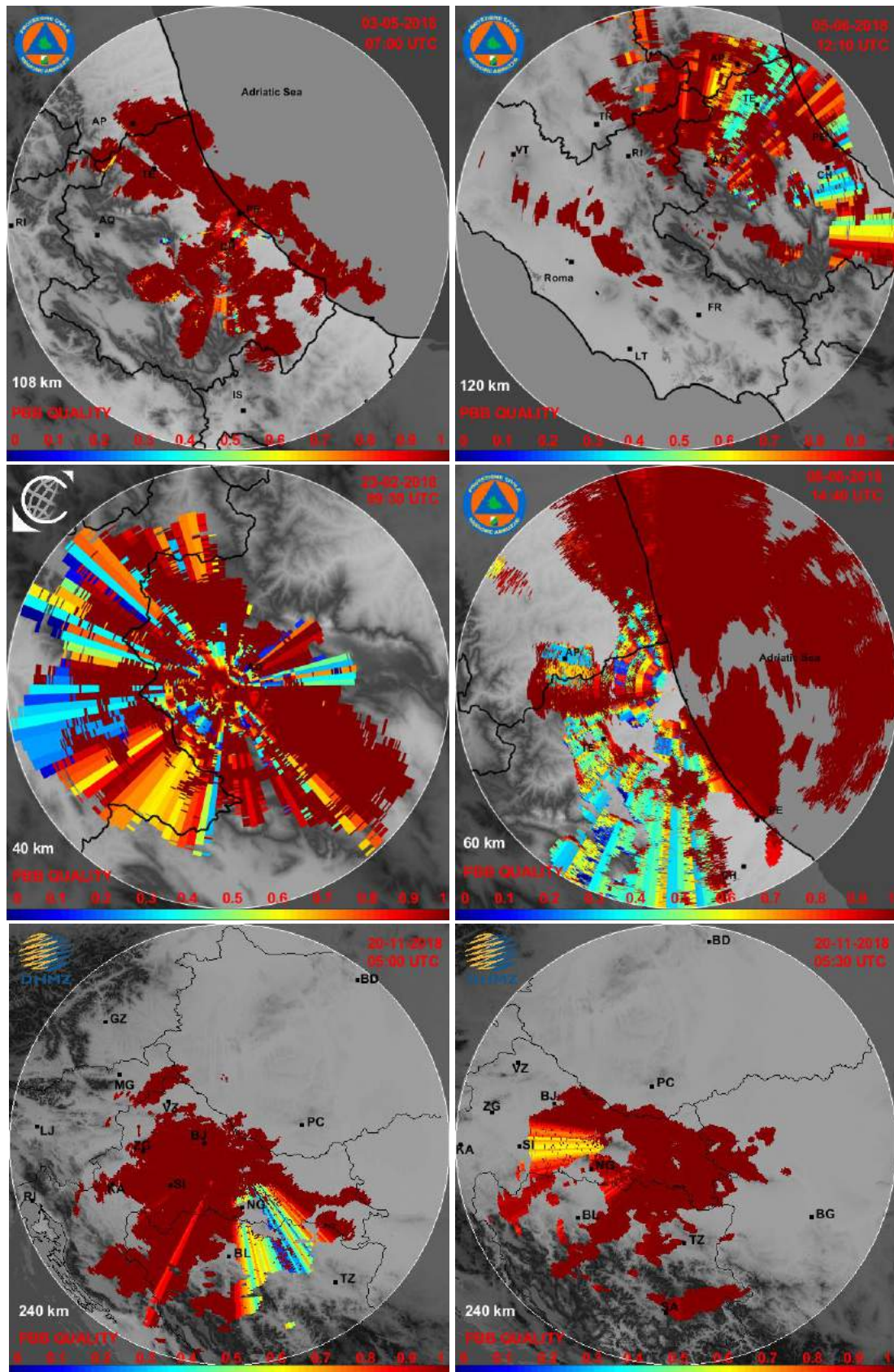


Figure 14 Examples of the PBB quality index (q_{PBB}) for Cepagatti (top left), Monte Midia (top right), L'Aquila (central left), Tortoreto (central right), Bilogora (bottom left) and Osijek (bottom right) radars

2.4.4 Long range measurement

The quality of radar data decreases with increasing distance from the radar, either because the beam broadens with the distance; the measurement comes from a larger volume and related averaging errors increase as well, or for the increasing height with respect to terrain. There is no possibility of correcting this effect. However, the data range-related deterioration can be determined quantitatively and taken into account in the related quality index. Following this approach [Friedrich, 2006], but introducing a square root, in order to ensure that quality does not drop too fast with the range distance, this index can be evaluated using a non-linear function [Rinollo, 2013]:

$$q_{RAN} = \begin{cases} 0.5 & \text{for } r \geq r_{max} \\ 1 & \text{for } r \leq r_{min} \\ \sqrt{\frac{r_{max} - r}{r_{max} - r_{min}}} & \text{for } r_{min} < r < r_{max} \end{cases}$$

where r_{max} can be set to maximum range of the radar and r_{min} can be set to zero (radar position). An example of the trend of the quality index as a function of the distance from the radar is shown in figure 15 up to 100 km.

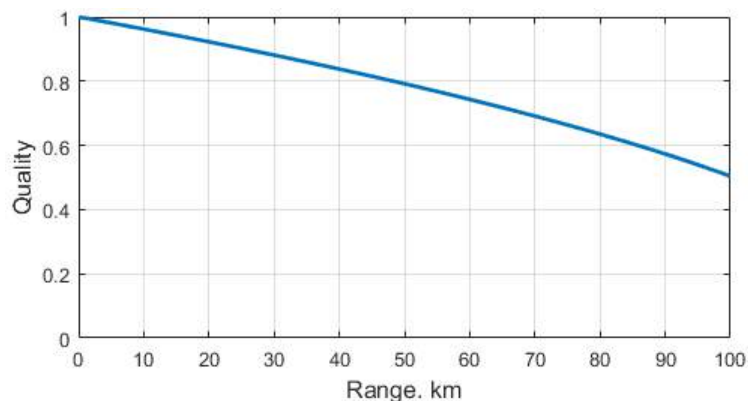


Figure 15 Example of the range quality index (q_{RAN}) profile for a radar with maximum range of 100 km

Figure 16 show some examples of the range quality index for various radar at different elevation angles.

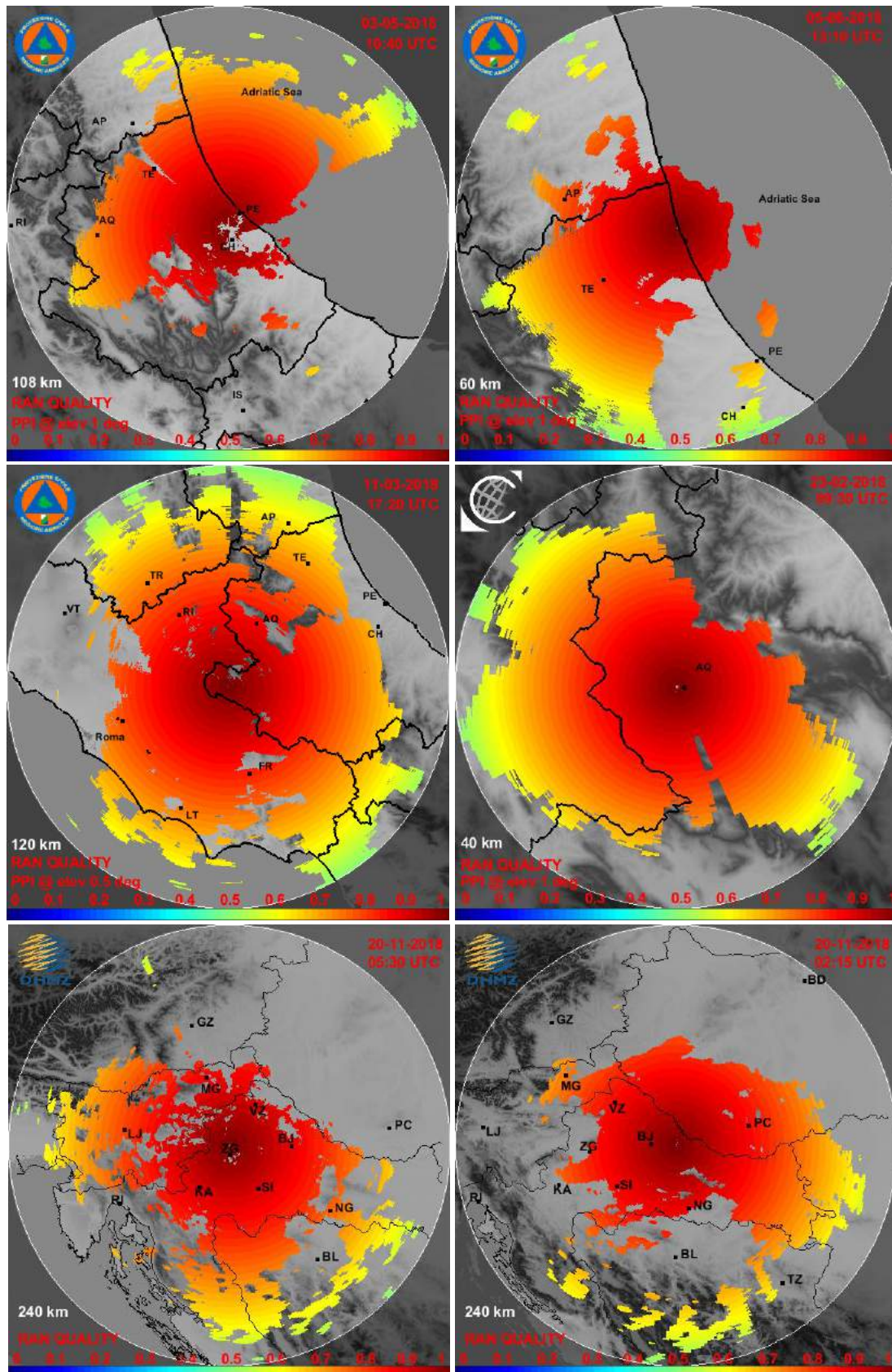


Figure 16 Examples of the range quality index (q_{RAN}) for Cepagatti (top left), Tortoreto (top right), Monte Midia (central left), L'Aquila (central right), Puntijarka (bottom left) and Bilogora (bottom right) radars

2.4.5 Rain path attenuation

Usually, for single or dual-polarization systems there are a variety of possible solutions of attenuation correction, based on the use of reflectivity and on differential phase shift when available, so it is recommended to evaluate the corrected reflectivity for quality as well. The magnitude of the attenuation in precipitation PIA (in dB), along the whole distance from the radar site to the given i -gate, can be considered as a quality factor for the given measurement gate i . Therefore, the relevant quality index q_{ATT} can be calculated from the formula [Barbieri, 2017]:

$$q_{ATT} = \begin{cases} 1 & \text{for } PIA < PIA_{min} \\ 0.5 & \text{for } PIA > PIA_{max} \\ \frac{2PIA_{max} - PIA_{min} - PIA}{2(PIA_{max} - PIA_{min})} & \text{for } PIA_{min} \leq PIA \leq PIA_{max} \end{cases}$$

where PIA_{min} and PIA_{max} are empirically determined depending of the features of each radar system. As an example, for the X-band radars we set $PIA_{min} = 3$ dB and $PIA_{max} = 15$ dB while for C-band radar, generally, smaller values are set.

In presence of events with fast and wide differential phase fluctuation (with polarimetric radars) or in general when there is high signal correction ($PIA > PIA_{max}$), the quality index is considered less reliable and reduced up to 50% (0.5).

Figure 17 shows a graphic representation of q_{ATT} as function of the PIA.

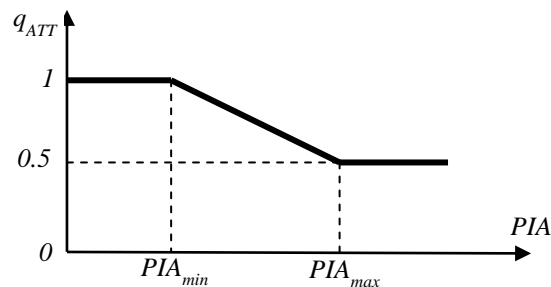


Figure 17 Attenuation quality index (q_{ATT}) as function of the PIA

Figure 18 shows some examples of the attenuation quality index.

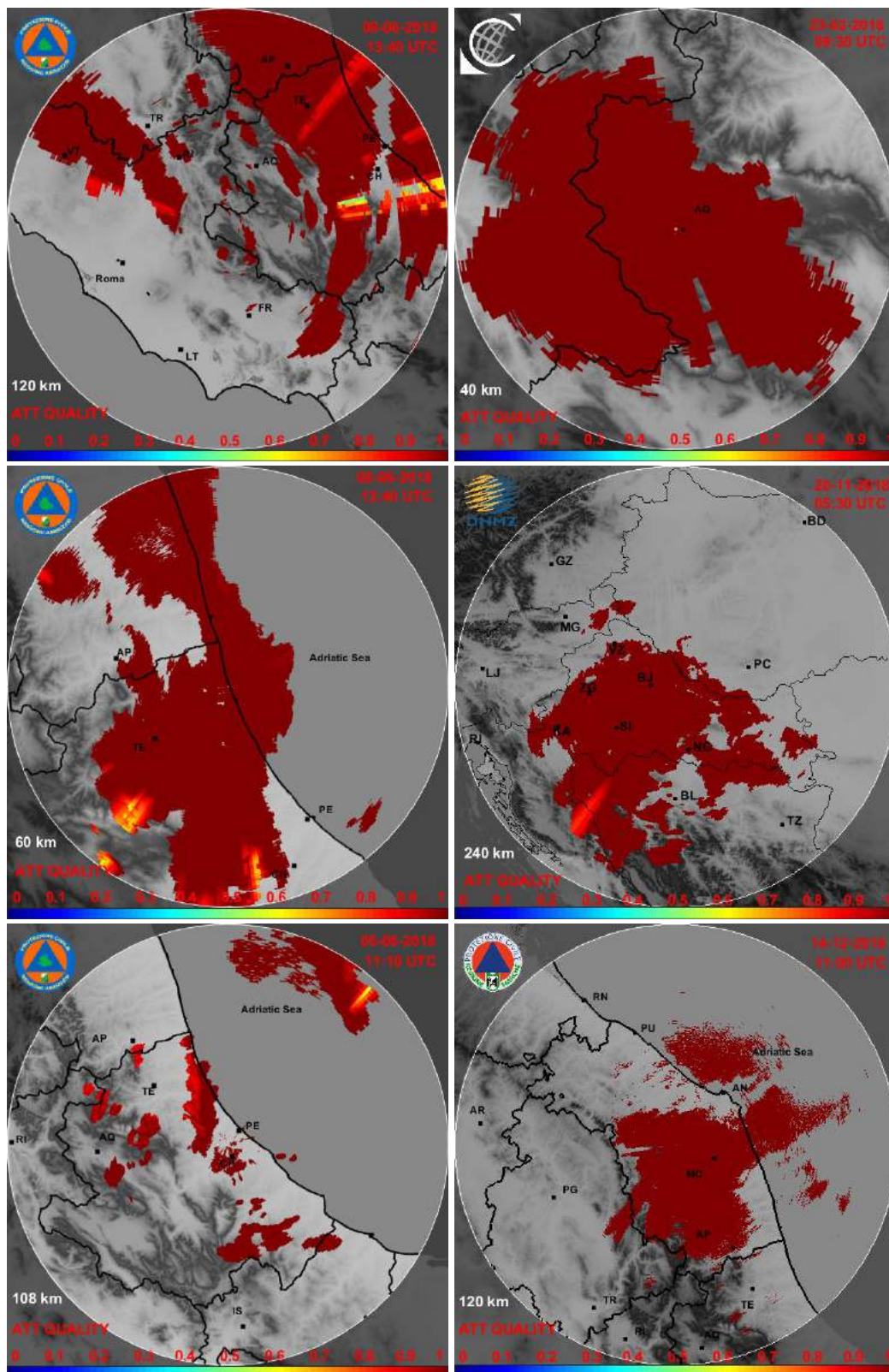


Figure 18 Examples of the attenuation quality index (q_{ATT}) for Monte Midia (top left), L'Aquila (top right), Tortoreto (central left), Bilogora (central right), Cepagatti (bottom left) and Cingoli (bottom right) radars

2.4.6 Inhomogeneous vertical profile of reflectivity

To mitigate radar precipitation errors due to non-uniform vertical profiles of reflectivity (VPR), and also due to the presence of the bright band, during stratiform precipitation, which causes significant overestimation in radar precipitation estimates, an appropriate correction should be applied.

The most important parameter that defines the vertical profile of reflectivity is the height of the freezing level. This value determines the position of the melting layer where, the vertical profiles of Z_h return intensified, exhibiting well-pronounced maxima.

Therefore, the identification of the melting layer is important not only for the VPR correction but it is also aimed at appraising the limit in distance or the height at which occurs for the rain attenuation correction.

The height of the freezing level is obtained from the vertical temperature profiles, derived from the measurements of radio sounding.

As a result of the storm vertical variability, the radar observations made at relatively high altitudes are not representative when estimating precipitation at ground level. In order to deal with such an issue, the reflectivity field can be projected onto the surface by estimating the vertical profile of reflectivity [Marzano, 2004]. Thus, after correction for VPR, the associated quality is assumed equal to 1. In case the compensation of this effect is not introduced, as in the RAMP chain, in the radar data, the quality index associated to VPR can be estimated as [Friedrich, 2006]:

$$q_{VPR} = \begin{cases} \frac{h_{+3dB} - h_{FL+200}}{2(h_{+3dB} - h_{-3dB})} & \text{for } h_{-3dB} < h_{FL+200} \text{ and } h_{+3dB} > h_{FL+200} \text{ and } h_{-3dB} > h_{FL-500} \\ 0.5 & \text{for } h_{-3dB} \geq h_{FL+200} \\ 1 & \text{for } h_{+3dB} \leq h_{FL-500} \\ 0 & \text{for } h_{-3dB} > h_{FL-500} \text{ and } h_{+3dB} < h_{FL+200} \\ \frac{h_{-3dB} - h_{FL-500}}{2(h_{-3dB} - h_{+3dB})} & \text{for } h_{-3dB} < h_{FL-500} \text{ and } h_{+3dB} > h_{FL-500} \end{cases}$$

where h_{FL} is the freezing layer height, $h_{+3dB} = h + \delta_{up}$, $h_{-3dB} = h - \delta_{dn}$, $\delta_{up} = r \sin(\phi) / \sin(\gamma + \phi)$, $\delta_{dn} = r \sin(\phi) / \sin(\gamma - \phi)$, $\phi = 0.5\Phi_{3dB}$ and $\gamma = \arctan((R+H_0) \cdot \cos(\theta)) / (r + (R+H_0) \cdot \sin(\theta))$.

Moreover, Φ_{3dB} is the 3 dB beam width and θ the antenna elevation angle while h is the height of the center of the radar beam computed with the relationship shown in section 2.2.

Figure 19 shows a representation of the q_{VPR} profile along a given azimuth and elevation angle for a case study. We can note that the q_{VPR} decreases significantly when it crosses the melting layer region, where the exterior of the ice crystals develops a water coating, and precipitation and ice crystals coexist. The index then slightly rises when it reaches and exceeds the freezing level.

Figure 20 shows examples of the q_{VPR} for different radars and in different temperature conditions. A higher temperature involves a higher altitude where the freezing level is present and a greater distance from the radar in which it is observed, especially for the beams at low elevations. This is shown in the figures by the size of the brown circles. The color change indicates the interception of the beam with the freezing level.

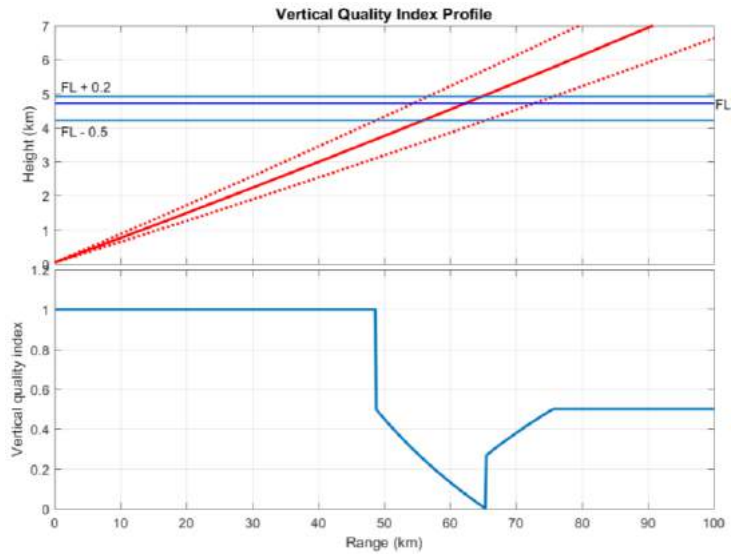


Figure 19 Scheme of the Vertical Quality index profile (q_{VPR}). FL indicate the height of the freezing level (about 4.75 km)

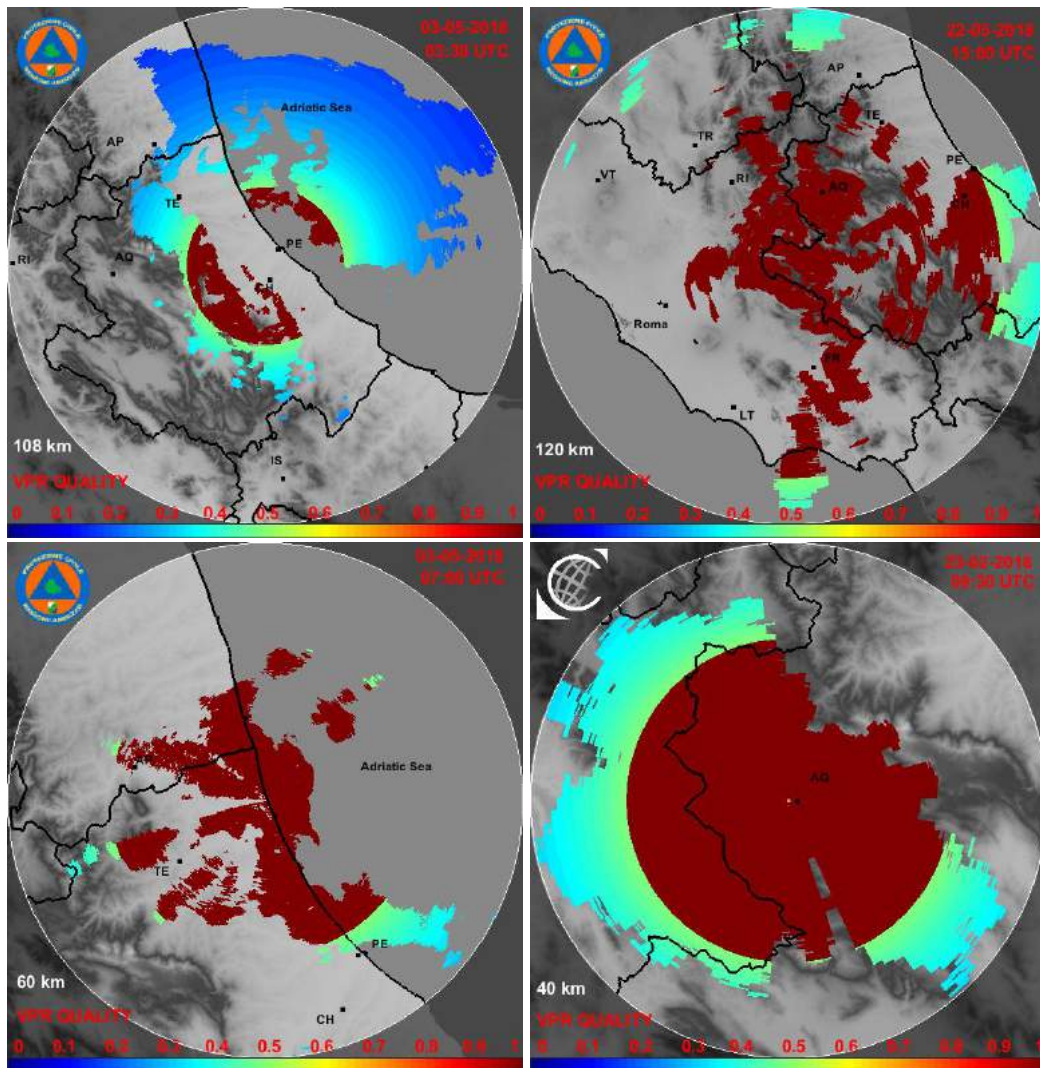


Figure 20 Examples of the vertical quality index (q_{VPR}) for different radars and events

2.5 Examples of application

Figure 21 shows the effect of the RAMP chain for the reflectivity data of the Monte Midia, Cepagatti and Tortoreto radars relating to precipitation events. It can be noted the elimination of some non-meteorological echoes and the attenuation correction. The corresponding maps of TQI are also shown once the individual quality indices defined by table 2 have been calculated.

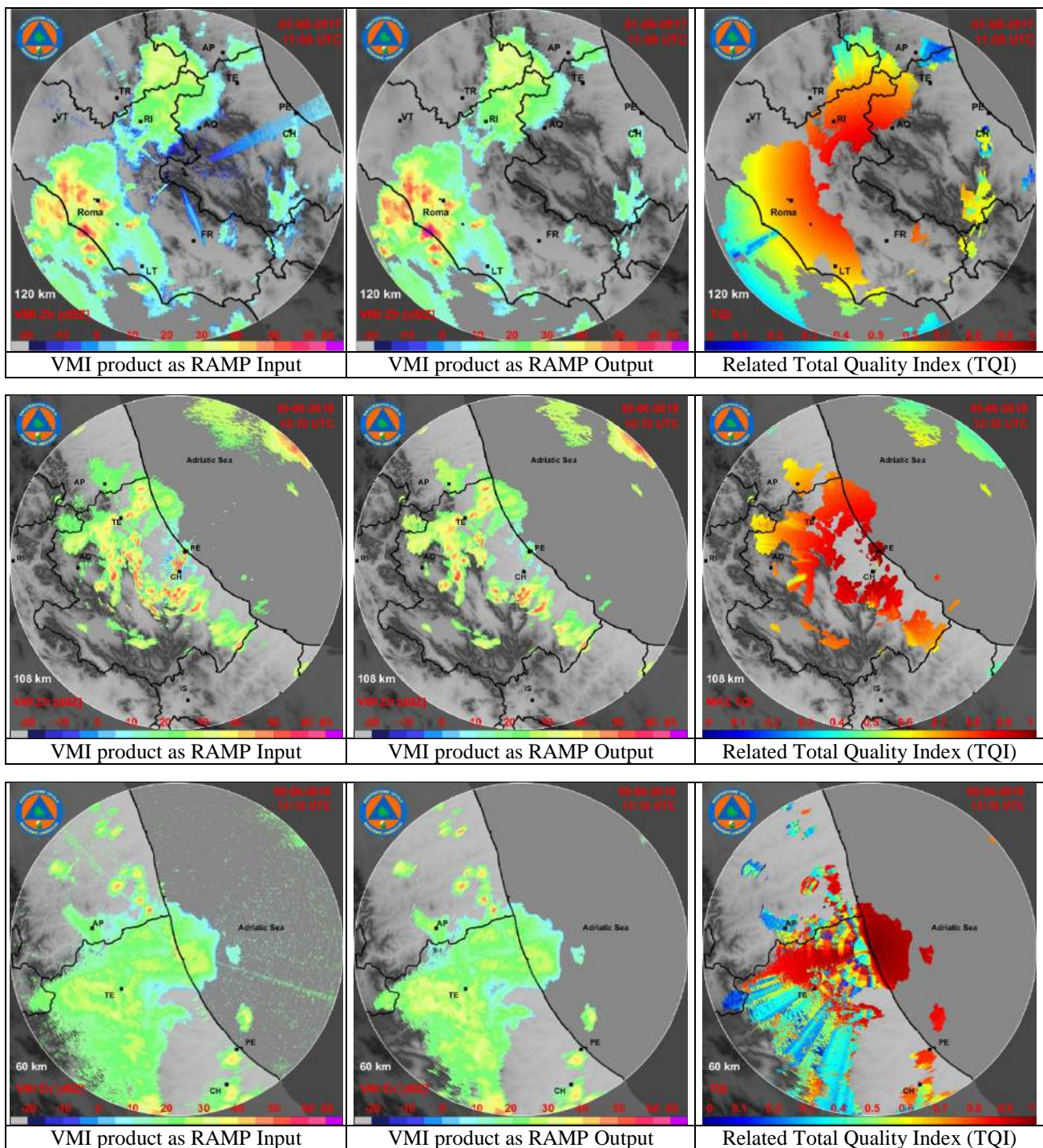


Figure 21 VMI products as input (left column) and output (central column) at RAMP chain for some events with precipitation for the Monte Midia (first row) Cepagatti (second row) and Tortoreto (third row) radars, the right column shows the overall quality matrices for the same events

Figure 22 shows the effect of the RAMP chain for the reflectivity data of the Cingoli, Osijek and Puntijarka radars relating to precipitation events. It can be noted the elimination of some non-meteorological echoes and the attenuation correction. The corresponding maps of TQI are also shown once the individual quality indices defined by table 2 have been calculated.

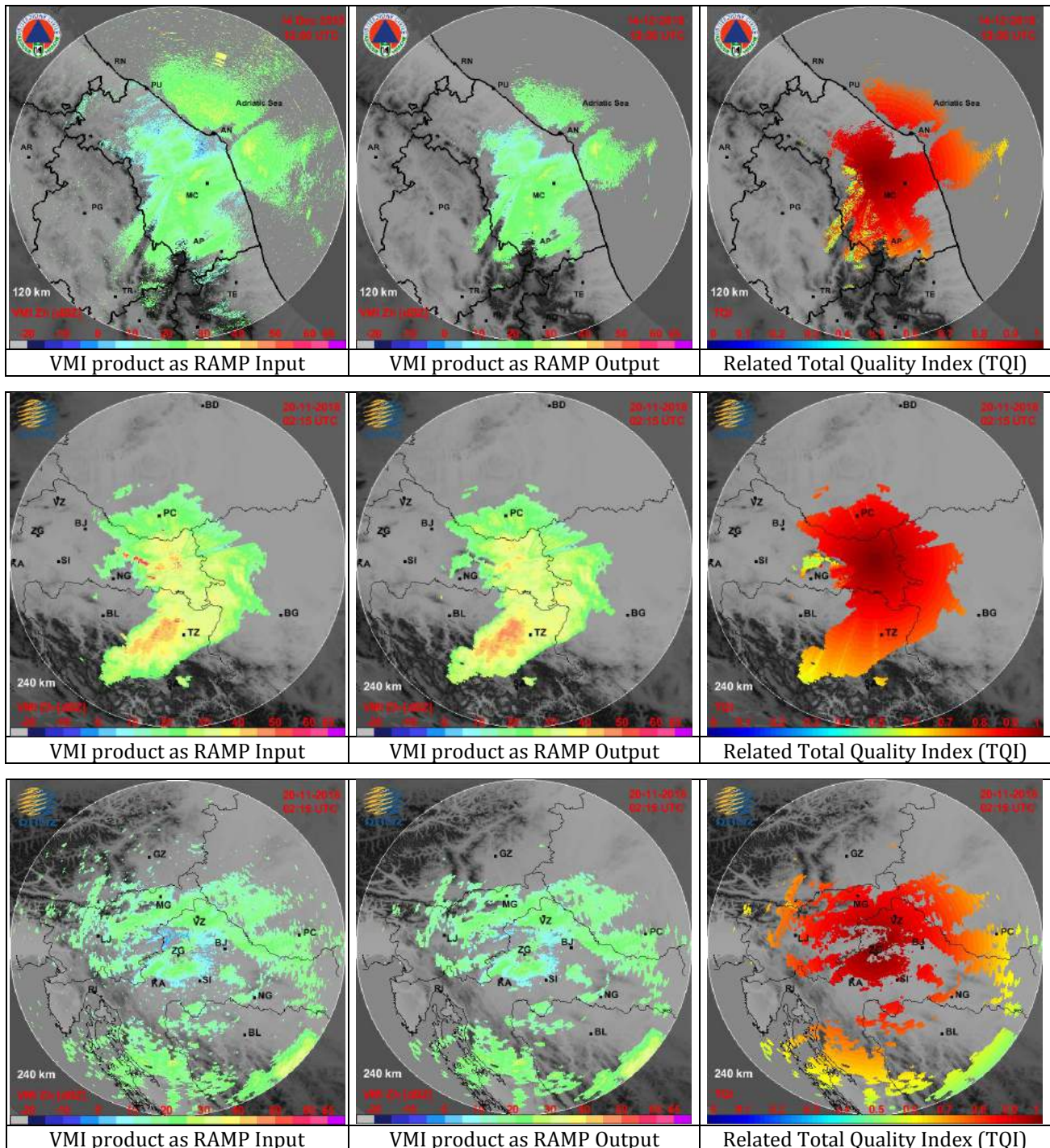


Figure 22 VMI products as input (left column) and output (central column) at RAMP chain for some events with precipitation for the Cingoli (first row), Osijek (second row) and Puntijarka (third row) radars, the right column shows the overall quality matrices for the same events

3. RADAR PRODUCTS FOR EXTREME WEATHER MONITORING

The next step, after error identification and correction performed by RAMP, is the generation of sophisticated radar products at single-radar level, in **figure 23** is recalled the part of the CRAMS chain assigned to this. Practically, the corrected volumes consist of sets of measurement gates organized in polar scans related to the rotation of an antenna at selected elevation angles. Based on the transfer from polar to Cartesian representations through a certain interpolation method the corrected volumes are processed to obtain various 2-D Cartesian products from single radar measurements dedicated to specific user requirements.

For AdriaMORE purpose, products focused on extreme events (described in **table 4**) have been taken into account, the standard algorithms for their generation are described in the next sections with some examples of application at the available radar data.

PRODUCT NUMBER	PRODUCT NAME	PRODUCT SYMBOL	SHORT DESCRIPTION
1	Maximum of reflectivity	VMI	This product is useful for a quick surveillance of regions of convective precipitation to locate both mature and newly developing thunderstorm
2	Convective storm detection	CSD	The product is aimed at distinguish stratiform and convective areas in the composite being the latter linked to the most intense and dangerous phenomena
3	Short time prediction of rainy field or nowcasting	NOW	The product is aimed at short-term forecast of convective cells motion
4	Precipitation estimation	SRI SRT	Precipitation products estimate the ground instantaneous (mm/h) and accumulated (mm) rain over radar coverage area. These products can issue warnings if the precipitation in a sub catchment region exceeds a threshold value
5	Vertically Integrated Liquid	VIL	The VIL value at a certain location is the sum of all observed radar reflectivities (converted to liquid water content) in a vertical column above this location. This product can be used as a measure for the potential strong rainfall
6	Hail detection	POH	The product is aimed at hail detection which is one of the most danger phenomena

Table 4 Brief description of the single-radar products implemented within CRAMS chain

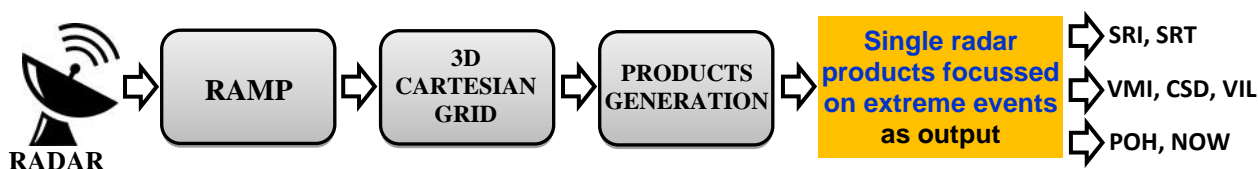


Figure 23 Part of the CRAMS chain devoted to the products generation at single-radar level

Product 1

MAXIMUM OF REFLECTIVITY

Short description

This product represents an image of the highest measured value of radar reflectivity Z (in dBZ) in each vertical column, it is called VMI (Vertical Maximum Intensity).

Allowing a complete vision of the potentially dangerous storm into volume scan, this product is useful for a quick surveillance of region of convective precipitation to locate both mature and newly developing thunderstorms, since storms that have only a small region of high intensity precipitations will show up the same as storms that have high intensity precipitations through a great depth.

Adopted Methodology

VMI products is the maximum value at each data column. It can be generated from polar as well as Cartesian data, in the figures 1.1 and 1.2 an example of generation from polar data is shown.

In figure 1.3 some examples of application on radar data are given.

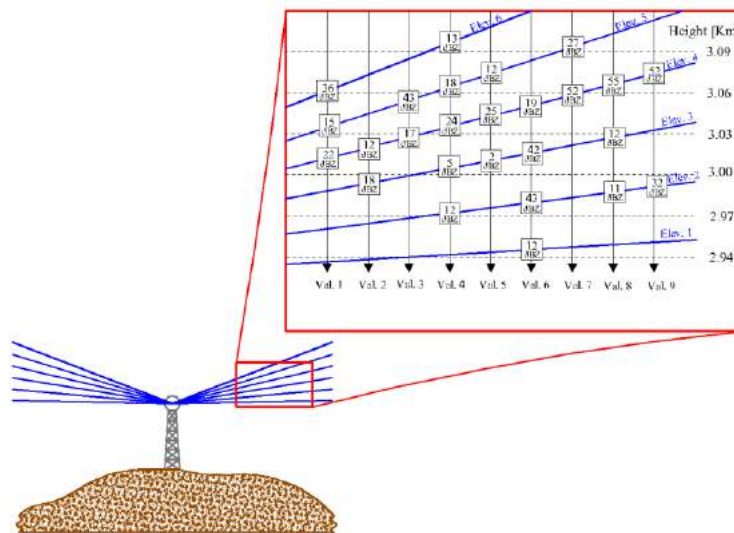


Figure 1.1 Section of radar volume with an example of reflectivity bin values

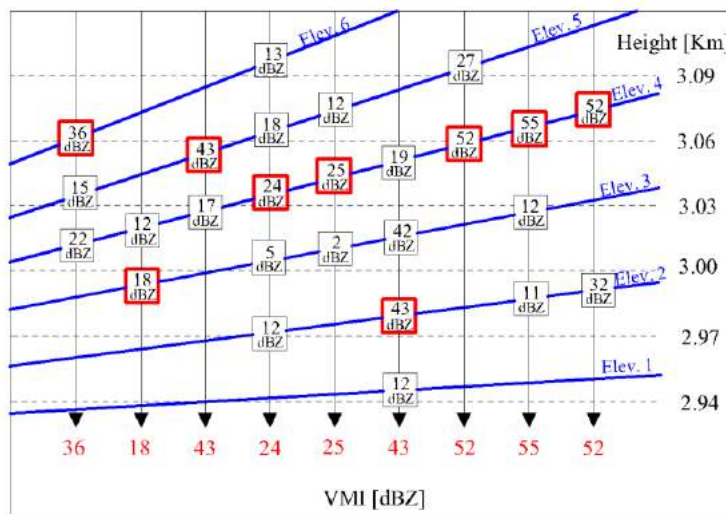


Figure 1.2 VMI product generation from polar data

Examples of application

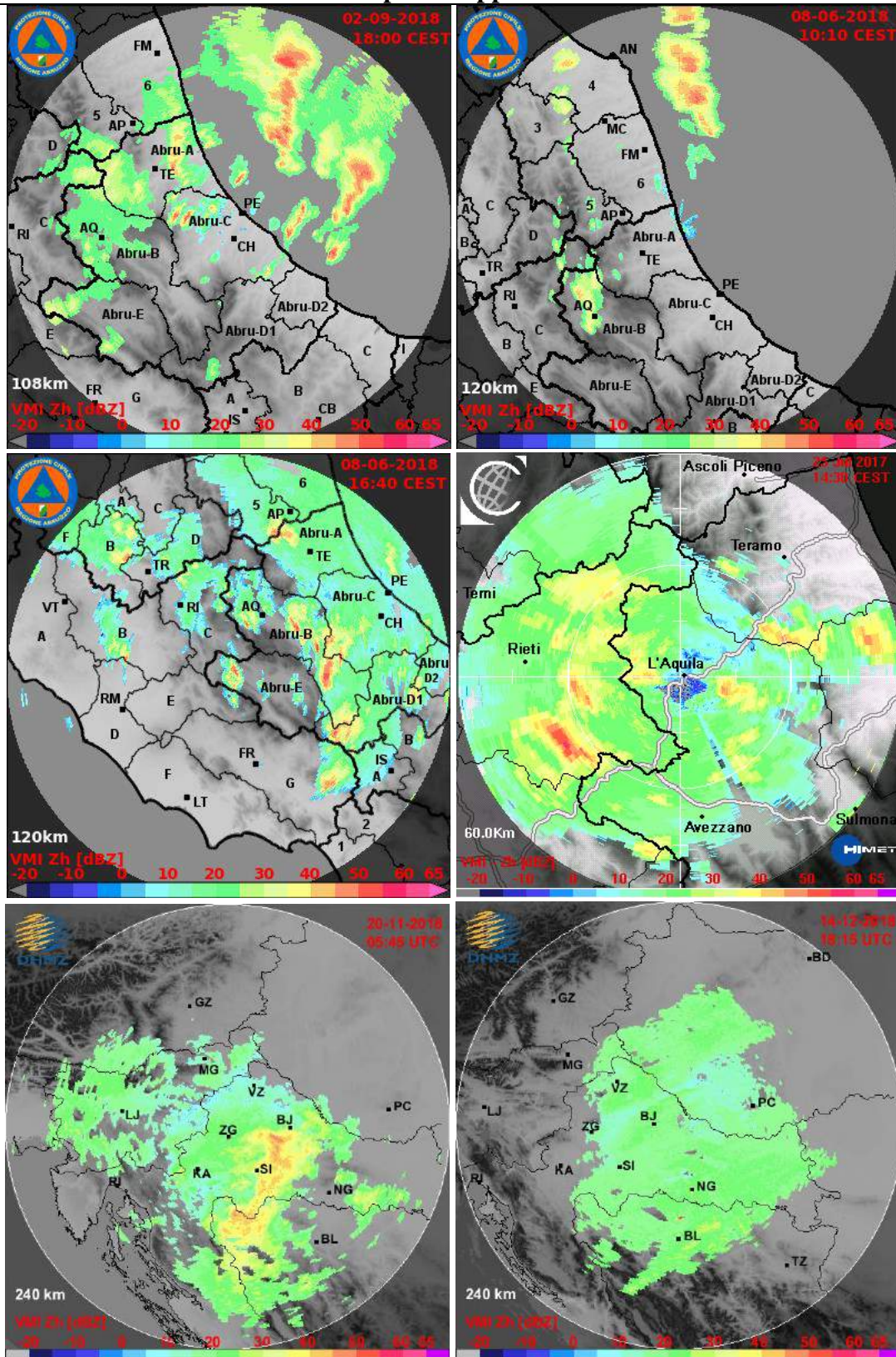


Figure 1.3 Examples of the VMI products for Cepagatti (top left), Tortoreto (top right), Monte Midia (central left), L'Aquila (central right), Puntijarka (bottom left) and Bilogora (bottom right) radars

Product 2

CONVECTIVE STORM DETECTION

Short description

Distinguishing between convective and stratiform is an important indicator of the vertical and horizontal structure of cloud systems producing precipitation. This precipitation identification product is aimed to provide a separation of the radar echoes into convective and stratiform regions, on the basis of the intensity and sharpness of the peaks of echoes intensity [Steiner, 1995]. An intermediate region, between the stratiform and convective is also introduced to indicate those events whose nature is uncertain.

Adopted Methodology

The method for the identification of precipitation type is based on the horizontal structure of precipitation field. The idea consists in the search of the reflectivity peaks: if they satisfy specific criteria, related to the ratio of the peak and the mean reflectivity of their immediate surroundings, they are classified as convective centers. The next step is classifying the area immediately adjacent as intermediate between stratiform and convective (mix) while the remaining reflectivity field is categorized as stratiform.

The criteria for the identification of convective centers and intermediate areas are based on the following steps:

- 1) *Intensity*: Any pixel in the radar reflectivity field characterized by a value of at least 40 dBZ is automatically labeled as a convective center, since rain of this intensity could practically never be stratiform;
- 2) *Peakedness*: Any pixel, in the radar reflectivity field, not identified as convective center in the first step, but which exceeds the average reflectivity of the surrounding area (Z_{bg}) of a certain difference in reflectivity (ΔZ), is also identified as convective center. Z_{bg} is determined according to a linear average of the nonzero radar echoes ($\text{mm}^6 \text{m}^{-3}$) within a distance of 11 km from the pixel. The relationship between ΔZ and Z_{bg} is represented by a continuous curve given by:

$$\Delta Z = \begin{cases} 15 & Z_{bg} < 0 \\ 15 - Z_{bg}^2/180 & 0 \leq Z_{bg} < 51,96 \\ 0 & Z_{bg} \geq 51,96 \end{cases}$$

and shown in figure 2.1.

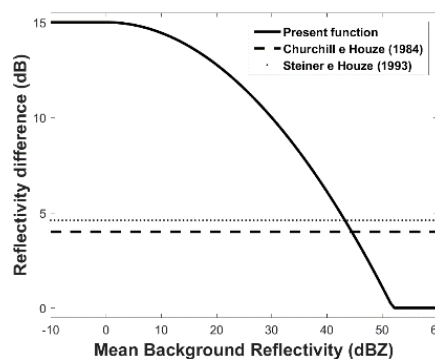


Figure 2.1 Peakedness criteria - reflectivity difference between a given pixel and mean background - used for convective center identification (solid curve). Points along and above this curve are classified as convective centers

- 3) *Surrounding area*: For each pixel identified as convective center by one of the above two criteria, all the surrounding pixels within an intermediate radius around that point, are classified as Mix centers and included in the intermediate area. The intermediate radius, expressed in [km], is also function of the mean reflectivity surrounding the convective center according to the relation of figure 2.2. Between those presented by [Steiner, 1995] the “medium” is used.

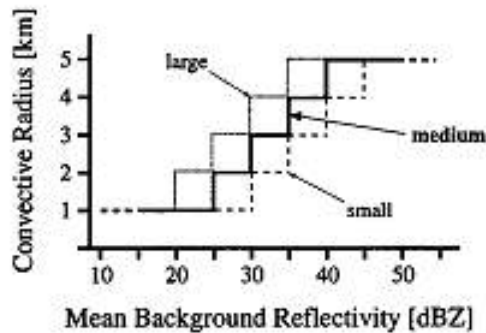


Figure 2.2 The convective area radius as a function of the mean background reflectivity

The just described method was subjected to slight changes, with the intent to preserve the results from errors due to spike reflectivity residues, generated by errors not corrected within the quality control. Below is shown a description of these changes, related to the first and second criterion.

- Once found the pixel which satisfies the condition defined by the first criterion (Intensity), is carried out the calculation of the mean reflectivity values measured within a distance of 2 km from it. If the reflectivity value of the pixel classified as convective exceeds a certain threshold, equal to the mean of the surrounding area added to twice the standard deviation of its reflectivity, then the pixel is classified as spike and is assigned the mean value of the background;
- The pixel which satisfies the condition expressed by the second criterion (peakedness) is compared with the mean value of the echoes measured within a distance of 5 km. If the reflectivity of the pixel exceeds a certain threshold, equal again to the mean value of the surroundings added to twice the standard deviation, then the pixel is classified as spike and is assigned the mean value of the surrounding area.

The output is constituted by a radar volume of indexes. Indexes represent a given precipitation type, the number of chosen classes is 3 and the legend for each of these classes is shown in table 2.1. Some examples of application are given in figure 2.3.

PRECIPITATION IDENTIFICATION			
Index	Acronym	Description	C
3	Conv	Convective	
2	Mix	Intermediate	
1	Strat	Stratiform	
0	NE	No Echo	

Table 2.1 Indexes and description for precipitation identification output

Examples of application

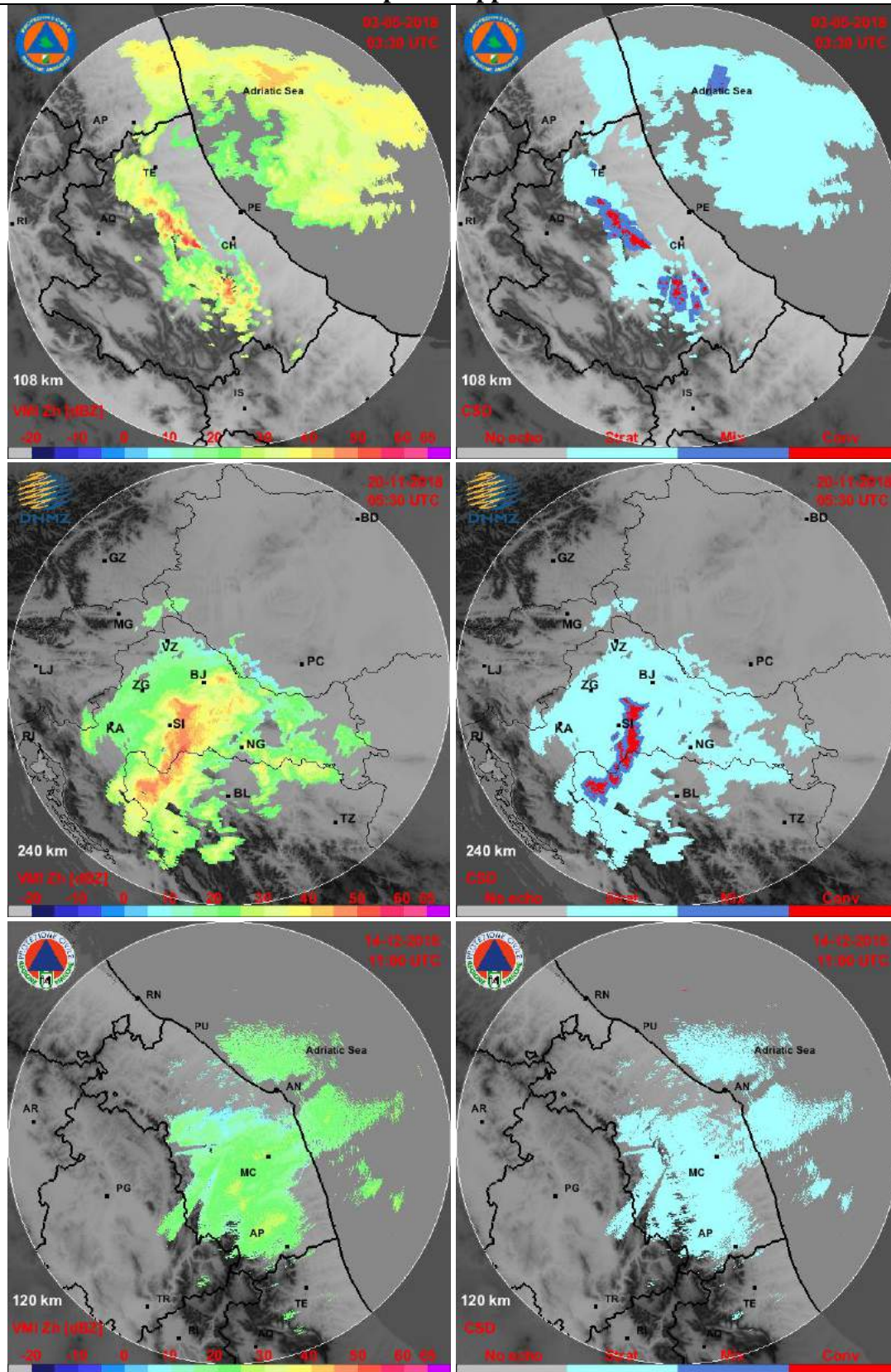
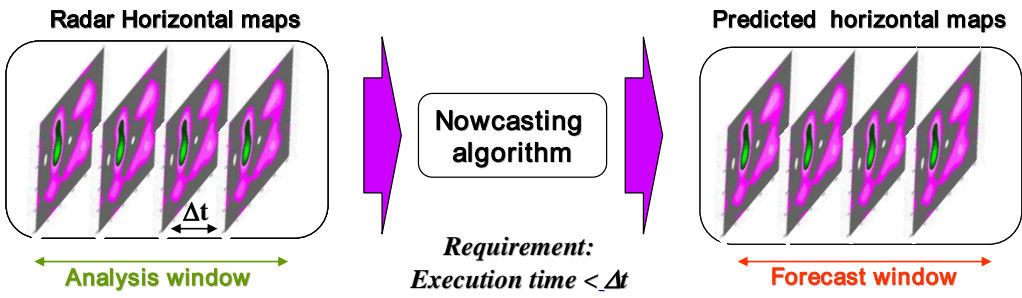


Figure 2.3 Example of convective cell identification: the VMI product (left panel) and the related classification (right panel) for Cepagatti (first row) Bilogora (second row) and Cingoli (third row) radars

Product 3	NOWCASTING
Short description	
<p>The nowcasting radar module is aimed to provide an indication of the temporal evolution of reflectivity or rain field at future instants in particular for convective cell storm. Due to high temporal variability of heavy rain cells (usually lasting for periods larger than the radar temporal resolution ΔT but less than 30 min), the nowcasting methods often propagate the information at short instants ahead, $t_0+n\cdot\Delta T$, with respect to the procedure initialization instant t_0.</p>	
Adopted Methodology	
<p>The nowcasting methodology adopted into CRAMS is based on the Spectral Pyramidal Advection Radar Estimator (SPARE) algorithm by [Montopoli, 2012]. The procedures take a temporal sequence of available radar maps and propagate the last available one in the future (see figure 3.1). The principle is based on the cross correlation between portions of two consecutive radar maps to compute the displacement vector between them [Kuglin, 1975]. The segmentation of each available radar field (also regarded as a special case of spatial decomposition) is a fundamental step which allows computing the displacement vectors for each identified portion of the radar maps. This implies that the resulting motion field is composed by several vector components (one for each identified portion of the radar map) that in principle are different each other. Thus, vortex or multiple system movements can be in principle caught.</p>	
<p>The original concept of SPARE algorithm, in its primordial version, is to perform spatial correlation on filtered radar images in the spectral domain of spatial frequency. The spatial filter used in the SPARE algorithm is able to isolate spatial components in a prescribed range of spatial scales. For this reason, SPARE is said to be pyramidal since the decomposition of radar maps in spatial components resemble a pyramid. This way to proceed tends to ensure a better estimation of the displacement field.</p>	
	
<p>Figure 3.1 Schematization of empirical nowcasting methodology. ΔT indicates the temporal resolution of radar scans</p>	
<p>The input variable for the radar nowcasting algorithm is the reflectivity at the two consecutive past instants with respect to procedure initialization t_0.</p>	
<p>Reflectivity factor at t_0</p>	<p>Z_{INP_2} [dBZ]</p>
<p>Reflectivity factor at $t_0-1\cdot\Delta T$</p>	<p>Z_{INP_1} [dBZ]</p>
<p>The output variables are the temporal sequence of predicted reflectivity fields:</p>	
<p>Reflectivity factor at $t_0+1\cdot\Delta T$</p>	<p>Z_{NOW_1} [dBZ]</p>
<p>Reflectivity factor at $t_0+2\cdot\Delta T$</p>	<p>Z_{NOW_2} [dBZ]</p>
<p>· · · · ·</p>	<p>· · · · ·</p>
<p>Reflectivity factor at $t_0+N\cdot\Delta T$</p>	<p>Z_{NOW_N} [dBZ]</p>
<p>The integer N drives the number of radar map to be predicted and indirectly indicates the maximum prediction period. Taking into account typical rain cell duration, a reasonable maximum prediction period is about 1 hour ahead from the current instant.</p>	
<p>In figure 3.2 three examples of application on radar data are given.</p>	

Examples of application

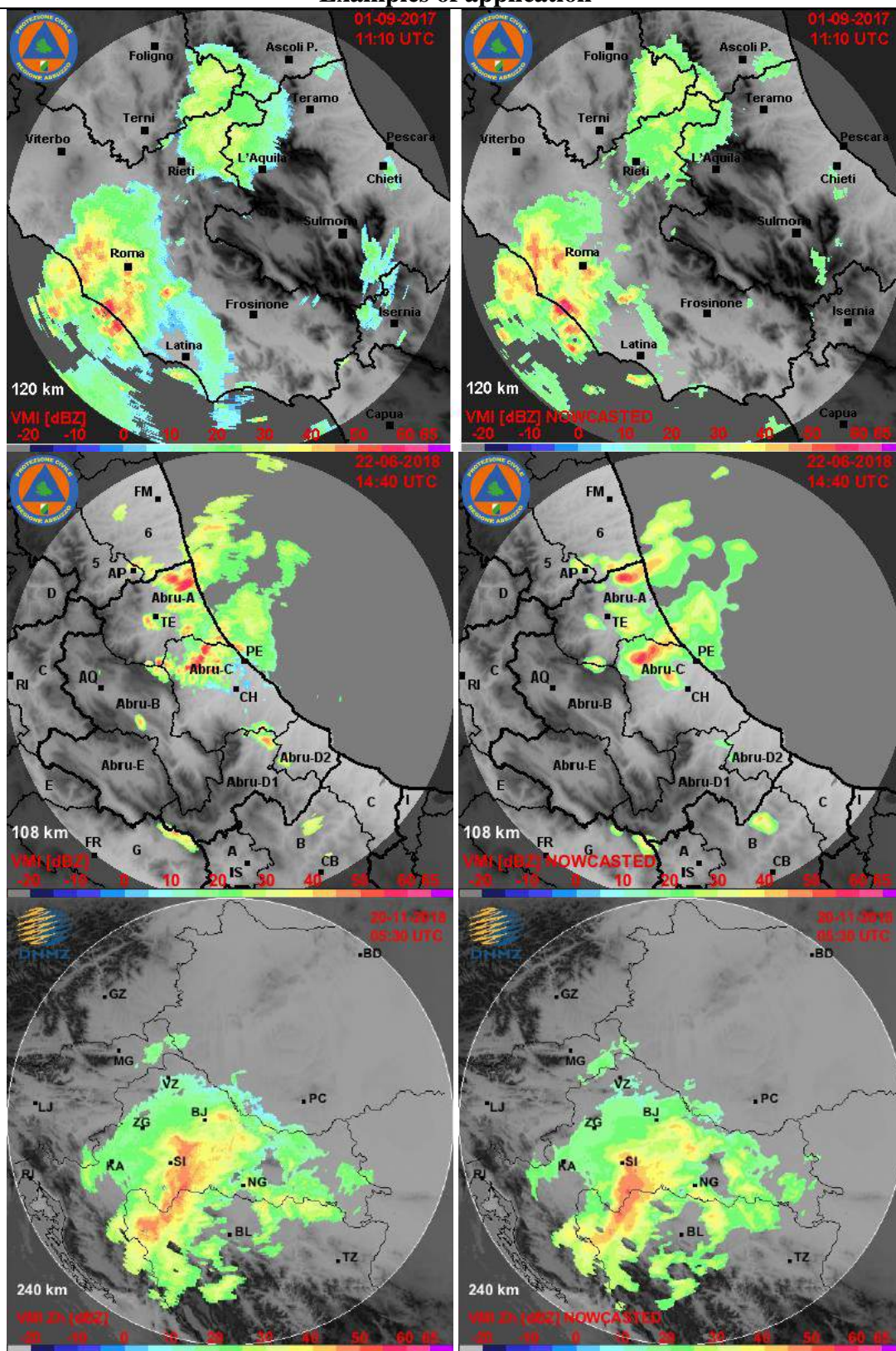


Figure 3.2 Examples of observed (left panel) and SPARE predicted (right panel) reflectivity maps for Monte Midia (first row) Cepagatti (second row) and Biligora (third row) radars

Product 4	PRECIPITATION ESTIMATION																					
Short description																						
<p>Accurate measurement of precipitation in terms of its intensity and location is important for both hydrological research and operational water management. The more traditional method of measuring rainfall with rain gauges is less expensive than weather radar, but only provides point measurements and offers limited information on spatial rainfall variability [Ciach, 2006; Koistinen, 1986]. Other instruments such as disdrometers [Joss, 1969] and microwave links [Leijnse, 2007] provide more insight in the microstructure and the spatial average, respectively, of precipitation. However, these instruments cannot capture the spatial variability of rainfall over larger areas such as river catchments. Radar systems offer a way of measuring areal precipitation with both a high spatial and temporal resolution and therefore currently offer the best solution to measure this spatial variability.</p> <p>Anyway radar-rainfall estimation is a complex process that involves several error sources, thus making its accurate estimation an extremely difficult task, in fact radar does not measure rainfall (SRI) directly but some related variable, e.g. radar reflectivity Z, for a single polarization system. For the conversion of radar reflectivity in the estimation of the intensity precipitation several forms of algorithms can be developed. Below is presented the most common approach, based mainly on a power-law algorithm [Park, 2005] that can be refined adopting a range dependent correction factor [Capozzi, 2014].</p>																						
Adopted Methodology																						
<p>The power-law algorithm presented below is a classical estimator of rainfall, it converts the radar reflectivity Z (expressed in dB) in the corresponding rainfall rate SRI (expressed in mm/h). Usually, the SRI (Surface Rainfall Intensity) at a given time i, can be express as:</p> $SRI_i = \left(10^{\frac{Zh}{10}} \right)^{1/b} \left(\frac{1}{a} \right)^{1/b} \quad (\text{mm/h})$ <p>with a and b coefficient depending of the type of the precipitation as well as the radar band (X, C or S). From the available SRI, the accumulated rain, named SRT (Surface Rainfall Total) can be computed, at a given time interval, as described below.</p> <p>The accumulated hourly precipitation, at time h, can be computed by the following relationship:</p> $SRT_{h,1} = \frac{1}{M} \sum_{i=1}^M SRI_i \quad (\text{mm})$ <p>where M represents the available SRIs in the hourly time interval.</p> <p>The accumulated precipitation between hours $h-N$ and h, or the cumulated at N hours from the current time h is equal to:</p> $SRT_{h,N} = \sum_{i=0}^{N-1} SRT_{h-i,1} \quad (\text{mm})$ <p>Find in the figures 4.1, 4.2 and 4.3 some examples of application, to be noted the color scale adopted with the rain thresholds that facilitates the reading of the maps (see table 4.1).</p>																						
<table border="1" style="width: 100%; border-collapse: collapse;"> <thead> <tr> <th style="background-color: #002060; color: white;">Thresholds</th> <th style="background-color: #002060; color: white;">Precipitation type</th> <th style="background-color: #002060; color: white;">Colour</th> </tr> </thead> <tbody> <tr> <td>0-6 mm/h</td> <td>weak</td> <td>shades of blue</td> </tr> <tr> <td>6-15 mm/h</td> <td>moderate</td> <td>shades of green</td> </tr> <tr> <td>15-35 mm/h</td> <td>strong</td> <td>shades of yellow</td> </tr> <tr> <td>35-70 mm/h</td> <td>very strong</td> <td>shades of purple</td> </tr> <tr> <td>70-150 mm/h</td> <td>violent</td> <td>shades of red</td> </tr> <tr> <td>> 150 mm/h</td> <td>storm</td> <td>shades of brown</td> </tr> </tbody> </table>		Thresholds	Precipitation type	Colour	0-6 mm/h	weak	shades of blue	6-15 mm/h	moderate	shades of green	15-35 mm/h	strong	shades of yellow	35-70 mm/h	very strong	shades of purple	70-150 mm/h	violent	shades of red	> 150 mm/h	storm	shades of brown
Thresholds	Precipitation type	Colour																				
0-6 mm/h	weak	shades of blue																				
6-15 mm/h	moderate	shades of green																				
15-35 mm/h	strong	shades of yellow																				
35-70 mm/h	very strong	shades of purple																				
70-150 mm/h	violent	shades of red																				
> 150 mm/h	storm	shades of brown																				
<p>Table 4.1 Precipitation thresholds and related colours in the maps</p>																						

Examples of application for SRI

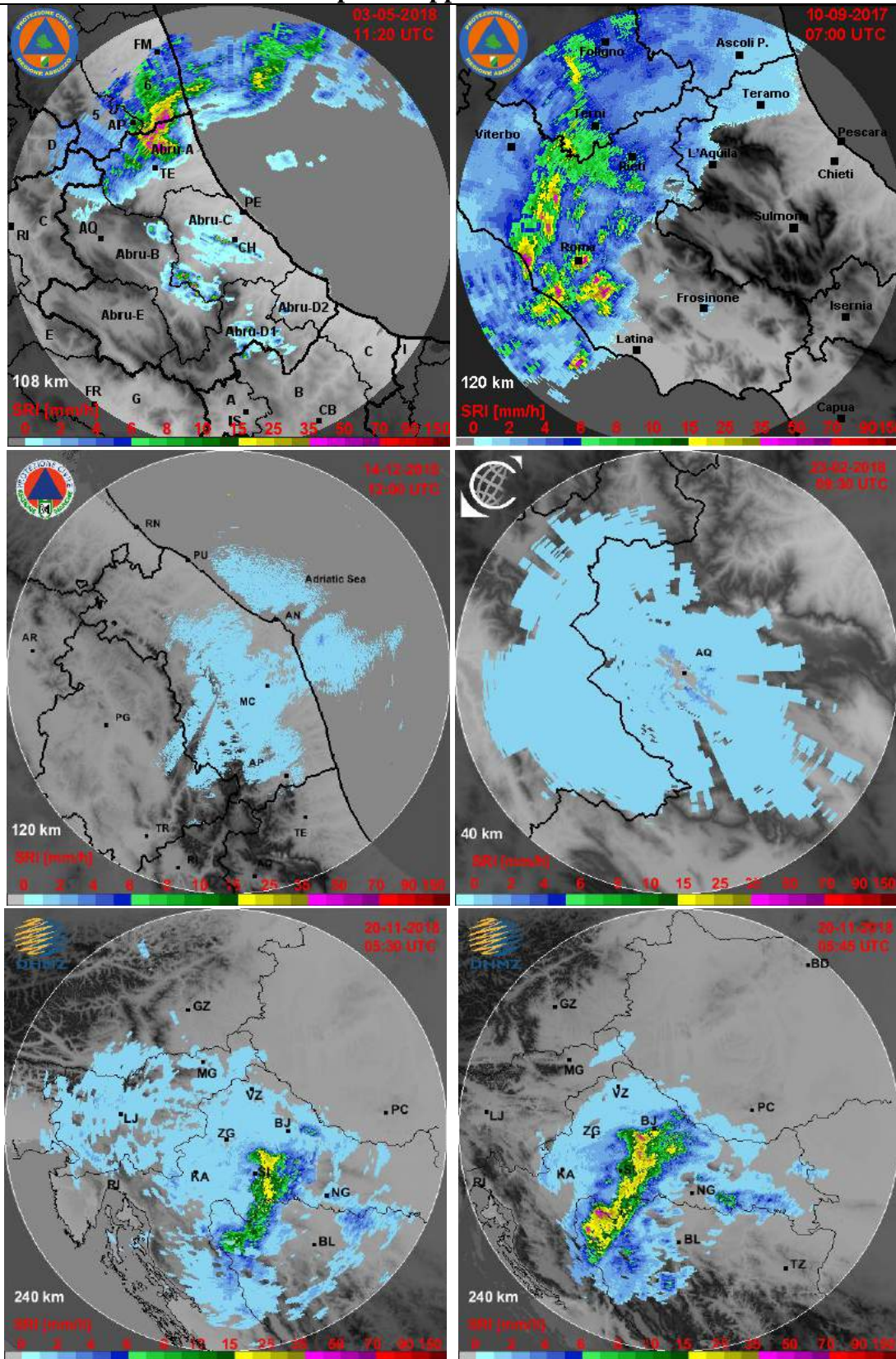


Figure 4.1 Examples of the instantaneous precipitation (SRI) for Cepagatti (top left), Monte Midia (top right), Cingoli (central left), L'Aquila (central right), Puntijarka (bottom left) and Bilogora (bottom right) radars

Examples of application for SRT

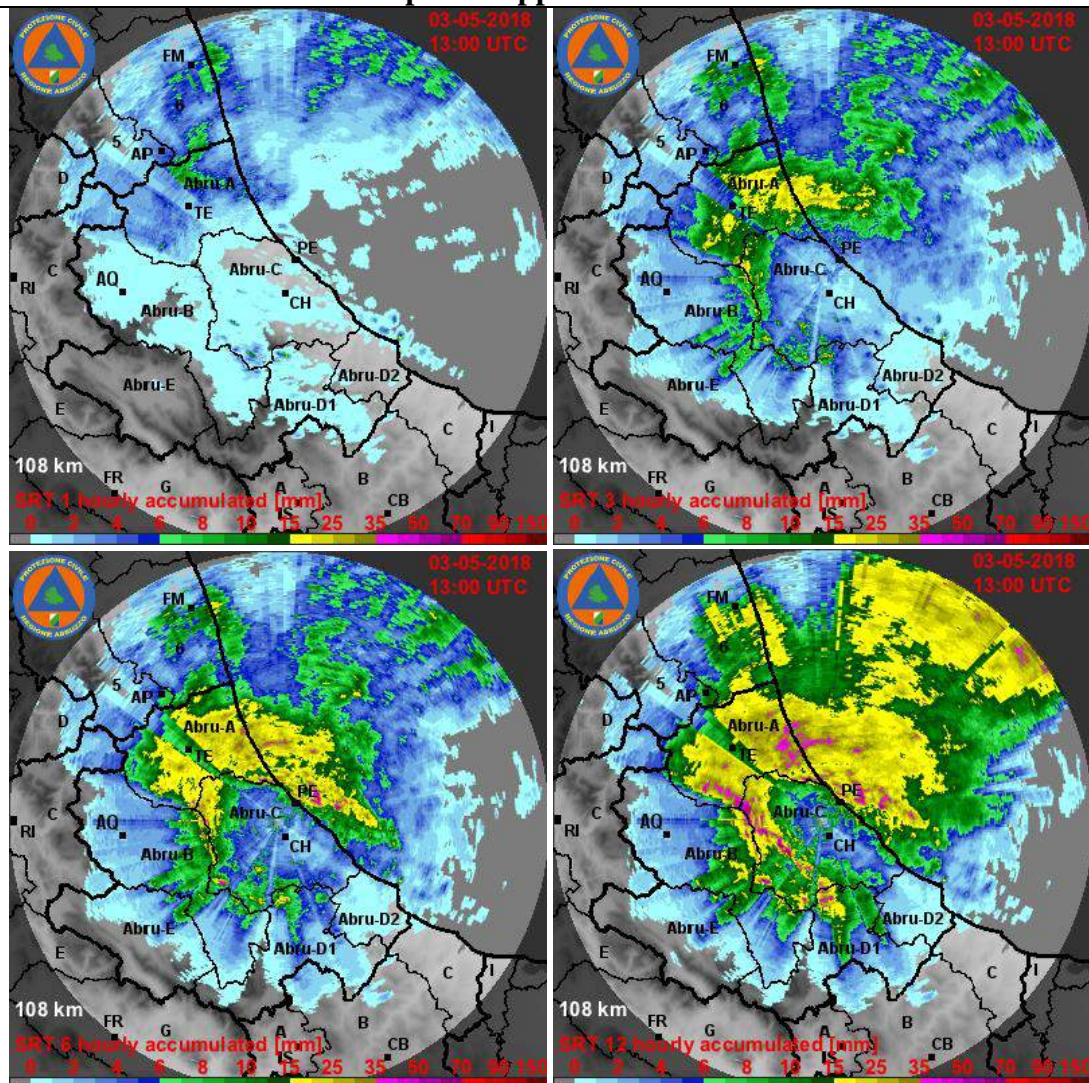


Figure 4.2 Examples of cumulated precipitation (SRT) for Cepagatti radar at 1, 3, 6 and 12 hours

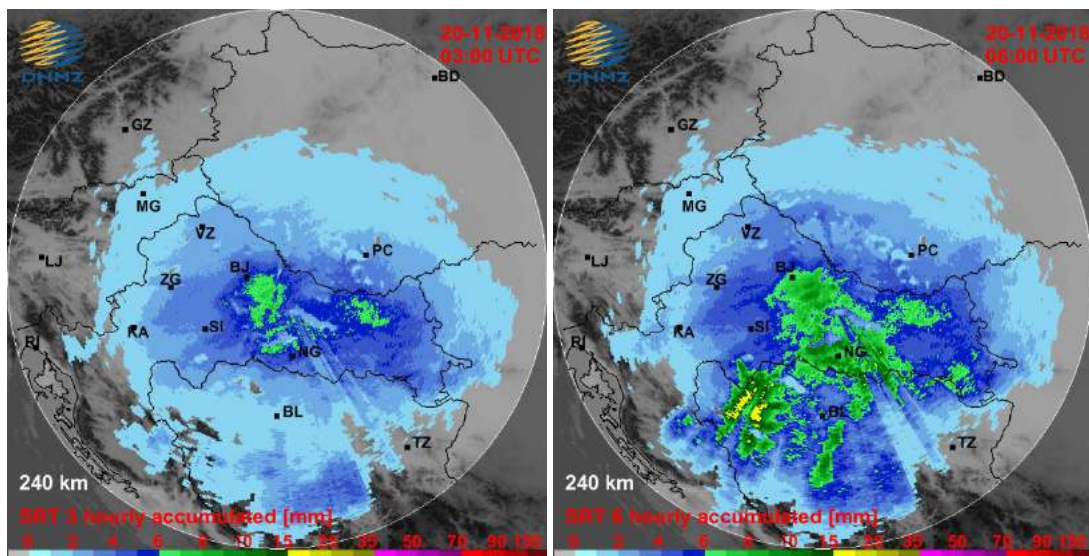


Figure 4.3 Examples of cumulated precipitation (SRT) for Biligora radar at 3 and 6 hours

Product 5

VERTICALLY INTEGRATED LIQUID

Short description

This product, called VIL (Vertically Integrated Liquid), is an excellent indicator of severe storm activity, especially with regard to the rainfall potential of a storm. The VIL shows the estimated water content contained within a user-defined layer. If the layer height is above the freezing level, high VIL values are an excellent indicator of severe storm and hail. If the layer height extends from the surface up to 3 km, then the VIL values serve as a forecasting guide as to how much precipitation is likely to fall during the next few minutes.

In general, it can be considered as a means of locating the most active and severe storms in a region, in stratiform situations VIL rarely exceeds a value of 10 kg/m², in thunderstorms, however, VIL is usually (much) higher.

When calculating VIL, have to be taken into consideration that VIL values in storms located too close to the radar will be underestimated, because the radar is not capable of scanning high enough to reach the upper portions of the storms.

Adopted Methodology

The VIL is estimated via conversion of the radar reflectivity to liquid-water content and subsequent vertical integration of this water content [Brimelow, 2004]. The three-dimensional radar data is converted to a plan-position indicator of the amount of liquid water present in a vertical column above a certain position.

VIL is calculated by vertically integrating reflectivity values from the top of a thunderstorm to the ground and converting reflectivity data into an equivalent liquid water content value. The general equation for VIL (expressed in kg/m²) is:

$$VIL = \sum_i a \left[\frac{(Z_i + Z_{i+1})}{2} \right]^b \Delta h$$

where Z_i and Z_{i+1} are two adjacent radar reflectivity bin values (expressed in mm⁶ m⁻³) at the same horizontal coordinate and Δh is the vertical distance between these i -th and the $i+1$ -th bin (expressed in meters).

Note that a and b coefficients depending on hydrometeor type, in this methodology two set of values are used: one for ice and one for rain, discern ice and rain is possible if freezing level is known.

This product can be generated from polar as well as Cartesian radar data, in the figure 5.1 an example of generation from polar data while in figure 5.2 examples of application on radar data are given.

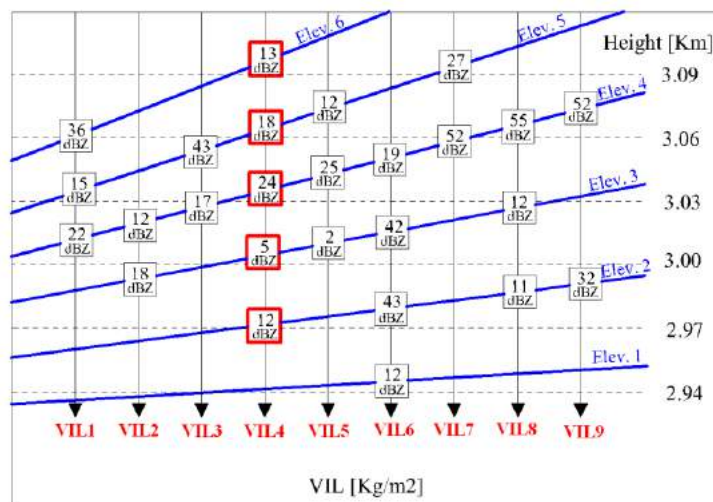
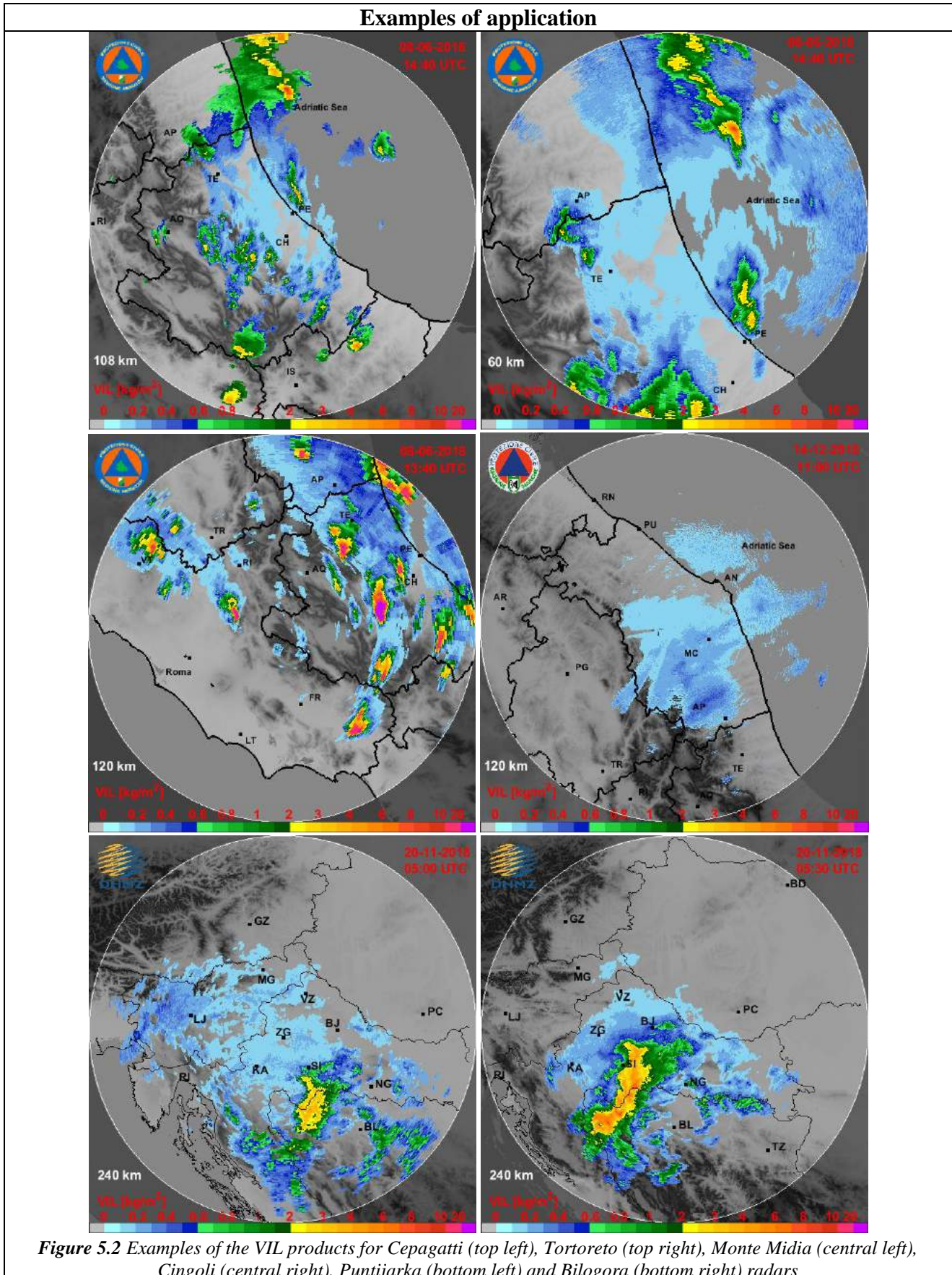


Figure 5.1 VIL product generation from polar radar data

Examples of application



Product 6	HAIL DETECTION
Short description	
<p>Hail events are typically related to crop losses, buildings and cars damages or casualties. Nowadays, the most direct way to distinguish between hail and rain is by using the dual polarization radar technique which can make a direct distinction between the spherical hailstones and the non-spherical rain droplets. However also single-polarization radar can be well used for hail assessment, in fact several methods are available from literature and some of them were tested by [Holleman, 2001]. Among these, for operational needs, the method that uses the value of VIL Density has been implemented in CRAMS chain.</p>	
Adopted Methodology	
<p>This method is based on VIL Density (VILD) calculation [Amburn, 1997]. VILD is simply the VIL divided by the EchoTOP and multiplied by 1000 in order to express the result as g/m^3. Remember that the EchoTOP is the height of the highest (in altitude) bin measured by radar during a volumetric scan. VILD makes VIL independent of height and then reduces error due to fact that VIL alone may not be sufficient to distinguish tall storms with low overall reflectivity (smaller targets, including possible small hail) from short storms with high reflectivity (larger targets including possible large hail). Thus, VILD is well adapt for the algorithms of hail detection.</p> <p>In other words, VIL Density is a parameter that “normalizes” the VIL using the height/depth (EchoTOP) of a thunderstorm, i.e., a bin's VIL is compared to the bin's EchoTOP. Therefore, VIL Density can be used to identify thunderstorms with high reflectivities relative to their height. Unlike VIL which usually increases as storms increase in height, VIL Density increases primarily due to increases in target size. Thus, as VIL Density increases, hail cores tend to be deeper, more intense, and reported hail sizes tend to be larger. Thunderstorms with larger VIL Density values generally produce larger hailstones at the surface. Usually VILD values ranges from 0 to $5 g \cdot m^{-3}$.</p> <p>Thus, VILD correlates well with storm cell containing hail cores, since those thunderstorms are usually characterized by high reflectivities at relatively high altitudes. This is, indeed, also a limitation of VILD algorithm since weather radars are not able to observe hail close to the ground. This problem may occur in circumstances of quite high freezing levels or if the hailstones fall through significant liquid water particles. To found a relationship between POH and VILD several thunderstorms with and without hail have to be examined in radar'. The probability of hail rises sharply as VILD increases and their relationship can be expresses, as an example, with a third-order polynomial fitted curve [Capozzi, 2018].</p>	
$POH = 100 \times (a_1 (VILD)^3 + a_2 (VILD)^2 + a_3 (VILD) + a_4)$	
<p>where a_i are regression coefficient and POH varies between 0 (no probability of hail) to 100 (certainty of hail).</p>	
<p>In figure 6.1 three examples of application on radar data are given.</p>	

Examples of application

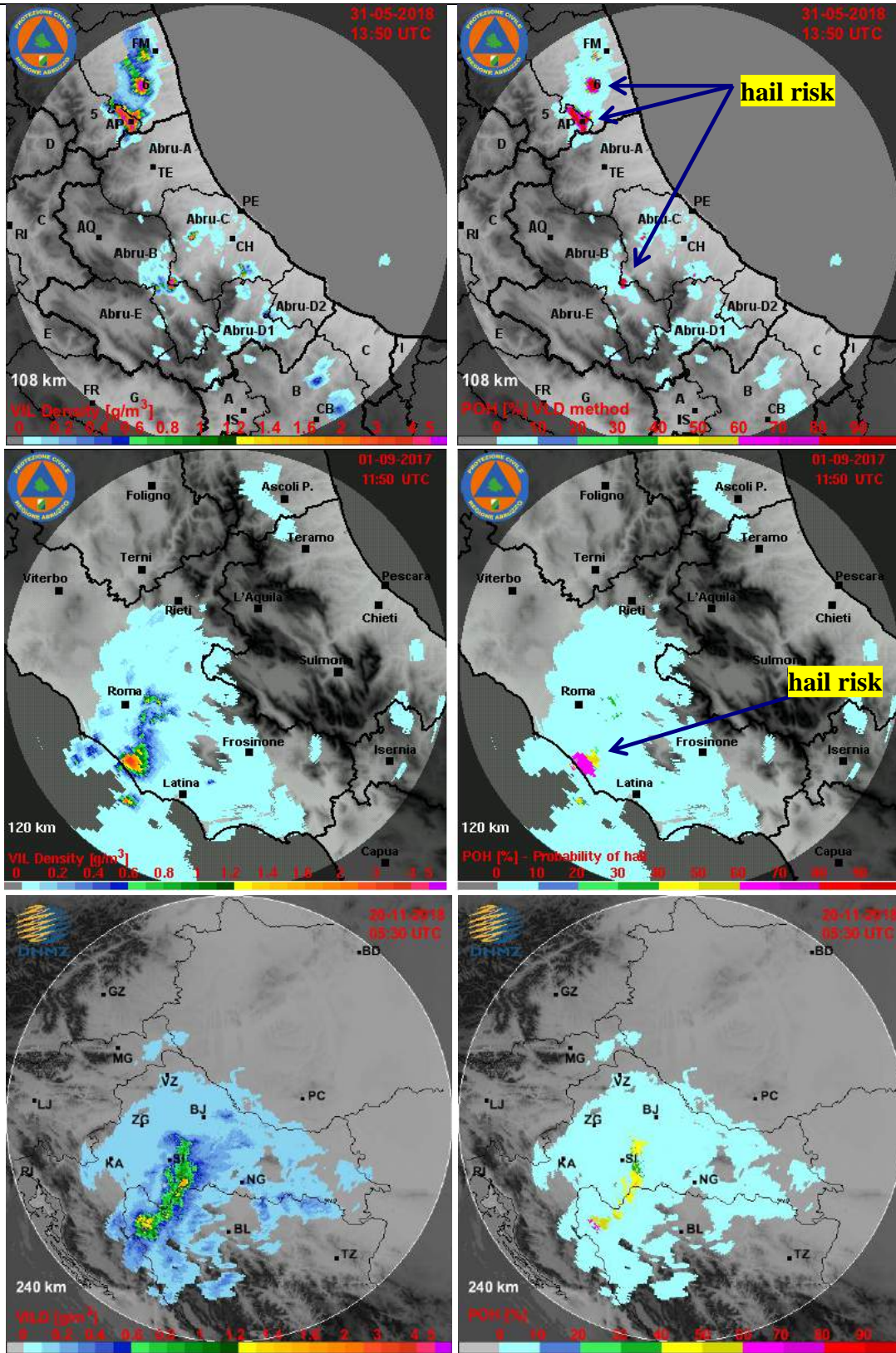


Figure 6.1 VIL density (left panel) and POH estimation (right panel) derived from Cepagatti (first row) M.Midia (second row) and Bilogora (third row) radars

4. REFERENCES

- **Amburn, S. A.,** and Wolf, P. L. “VIL Density as a Hail Indicator”, *Wea. Forecasting*, 12, 473-478, **1997**
- **Barbieri, S.** “Testing of dual-polarization processing algorithms for radar rainfall estimation in tropical scenarios”, HSAF, Visiting Scientist H_AS17_01 report, **2017**
- **Barbieri, S.,** Picciotti, E., Montopoli, M., Di Fabio, S., Lidori, R., Marzano, F. S., Kalogiros, J., Anagnostou, M. and Baldini, L. “ Intercomparison of dual-polarization X-band miniradar performances with reference radar systems at X and C band in Rome supersite” *Proc. ERAD2014*, Garmisch-Partenkirchen (Germany), 1-5 September **2014**
- **Battan, L. J.** “Radar observation of the atmosphere”, University of Chicago Press, ISBN 9780226039190, Chicago – London, UK, **1973**
- **Bebbington, D.,** Rae, S., Bech, J., Codina, B. and Picanyol, M. “Modelling of weather radar echoes from anomalous propagation using a hybrid parabolic equation method and NWP model data”, *Natural Hazards and Earth System Sciences*, Vol. 7, pp. 391–398, ISSN 1561-8633, **2007**
- **Bech, J.,** Codina, B., Lorente, J. and Bebbington, D. “The sensitivity of single polarization weather radar beam blockage correction to variability in the vertical refractivity gradient”, *J. Atmos. Oc. Tech.*, vol. 20, pp. 845-855, **2003**
- **Bech, J.,** Gjertsen U., Haase G. “Modelling weather radar beam propagation and topographical blockage at northern high latitudes”. *Q. J. R. Meteorolog. Soc.* 133: 1191–1204. **2007**
- **Brimelow, J. C.,** Reuter, G. W., Bellon, A. and Hudak, D. “A radar-based methodology for preparing a severe thunderstorm climatology in central Alberta”, *Atmosphere-Ocean*, 42:1, 13-22, DOI: 10.3137/ao.420102, **2004**
- **Bringi, V. N.** and Chandrasekar, V. “Polarimetric Doppler Weather Radar: Principles and Applications”, Cambridge, UK, Cambridge University Press, **2001**
- **Capozzi, V.,** Picciotti, E., Mazzarella, V., Marzano, F. S. and Budillon, G. “Fuzzy-logic detection and probability of hail exploiting short-range X-band weather radar”, *Atmospheric Research*, Volume 201, Pages 17-33, <https://doi.org/10.1016/j.atmosres.2017.10.006>, March **2018**
- **Capozzi, V.,** Picciotti, E., Budillon, G., and Marzano, F. S. “X-band weather radar monitoring of precipitation fields in Naples urban areas: data quality, comparison and analysis”, *Proc. ERAD2014*, Garmisch-Partenkirchen (Germany), 1-5 September **2014**
- **Ciach, G. J.** and Krajewski, W. F. “Analysis and modeling of spatial correlation structure of small-scale rainfall in Central Oklahoma”, *Adv. Water Resour.*, 29, 1450–1463, **2006**
- **Collier, C. G.** “Applications of weather radar systems”, A guide to uses of radar data in meteorology and hydrology. Wiley-Praxis, ISBN 0-7458-0510-8, Chichester, UK, **1996**
- **Doviak, R. J.,** and Zrnica, D. S. “Doppler Radar and Weather Observations”, Academic Press, **1993**
- **Einfalt, T.** and Michaelides, S. “Quality control of precipitation data”, In: *Precipitation: Advances in measurement, estimation and prediction*, S. Michaelides, (Ed.), 101–126, Springer-Verlag, Berlin – Heidelberg, Germany, **2008**
- **Fornasiero, A.,** Alberoni, PP., Amorati, R., Ferraris L., Taramasso, A. C. “Effects of propagation conditions on radar beam-ground interaction: impact on data quality”, *Adv. Geosci.* 2: 201–208, **2005**

- **Franco, M.**, Sempere-Torres, D., Sánchez-Diezma, R. and Andrieu, H. “A methodology to identify the vertical profile of reflectivity from radar scans and to estimate the rainrate at ground at different distances”, *Proc. ERAD 2002*, 299–304, **2002**
- **Friedrich, K.**, Hagen, M., and Einfalt, T. “A quality control concept for radar reflectivity, polarimetric parameters, and Doppler velocity”, *J. Atmos. Ocean. Tech.*, 23, pp. 865–887, **2006**
- **Fulton, R. A.**, Breidenbach, J. P., Seo, D., Miller, D. and O’Bannon, T. “The WSR-88D rainfall algorithm”. *Wea. Forecasting*, 13, 377–395, **1998**
- **Gekat, F.**, Meischner, P., Friedrich, K., Hagen, M., Koistinen, J., Michelson, D. B. and Huuskonen, A. “The state of weather radar operations, networks and products”, In: *Weather radar. Principles and advanced applications*, P. Meischner, (Ed.), 1–51, Springer-Verlag, ISBN 3-540-000328-2, Berlin – Heidelberg, Germany, **2004**
- **Germann, U.** and Joss, J. “Operational measurement of precipitation in mountainous terrain”, In: *Weather radar. Principles and advanced applications*, P. Meischner, (Ed.), 52– 77, Springer-Verlag, ISBN 3-540-000328-2, Berlin – Heidelberg, Germany, **2004**
- **Goltz, C.**, Einfalt, T. and Galli, G. “Radar data quality control methods in VOLTAIRE”, *Meteorologische Zeitschrift*, Vol. 15, pp. 497–504, ISSN 1610-1227, **2006**
- **Gourley, J. J.**, Tabary, P. and Parent du Chatelet, J. “Empirical estimation of attenuation from differential propagation phase measurements at C-band”, *J. Appl. Meteorol. Climatol.*, Vol. 46., pp. 306 – 317, **2007**
- **Holleman, I.**, Michelson, D., Galli, G., Germann, U. and Peura, M. “Quality information for radars and radar data. OPERA workpackage 1.2 (OPERA_2005_19 document)”, **2006**
- **Holleman, I.** “Hail detection using single-polarization radar”, Scientific Report, KNMI WR 2001-01, **2001**
- **Illingworth, A.** “Improved precipitation rates and data quality by using polarimetric measurements”, In: *Weather radar. Principles and advanced application*, P. Meischner, Ed.), 130–166, Springer-Verlag, ISBN 3-540-000328-2, Berlin – Heidelberg, Germany, **2004**
- **Joss, J.** and Waldvogel, A. “Raindrop size distribution and sampling size errors”, *J. Atmos. Sci.*, 26, 566–569, **1969**
- **Koistinen, J.** and Puhakka, T. “Can we calibrate radar with raingauges”, *Geophysica*, 22 (1-2), 119–129, **1986**
- **Kuglin, C.** and Hines, D. “The Phase Correlation Image Alignment Method,”, *Proc. Int. Conf. Cybernetics and Society*, pp. 163-165, **1975**
- **Leijnse, H.**, Uijlenhoet, R., and Stricker, J. N. M. “Hydrometeorological application of a microwave link: 2. precipitation”, *Water Resour. Res.*, 43, W04417, doi:10.1029/2006WR004989, **2007**
- **Maki, M.**, Maesaka, T., Kato, A., Kim, D. S and Iawanami, K. “Developing a composite rainfall map based on observations from an X-band polarimetric radar network and conventional C-band radar”, *NISCAIR-CSIR, India*, vol. 41, pp. 461-470, August **2012**
- **Marzano, F. S.**, Picciotti, E. and Vulpiani, G. “Rain field and reflectivity vertical profile reconstruction from C-band radar volumetric data”, *IEEE Trans. Geosci. Rem. Sens.*, vol. 42, n. 4, pp. 1033-1046, **2004**
- **Meischner, P.** “Weather radar. Principles and advanced applications”, Springer- Verlag, ISBN 3-540-000328-2, Berlin – Heidelberg, Germany, **2004**

- **Michelson, D.**, Einfalt, T., Holleman, I., Gjertsen, U., Friedrich, K., Haase, G., Lindskog, M. and Jurczyk, A. “Weather radar data quality in Europe – quality control and characterization”, Review. COST Action 717, ISBN 92-898-0018-6, Luxembourg, **2005**
- **Montopoli, M.**, Marzano, F. S., Picciotti, E. and Vulpiani, G. “Spatially-Adaptive Advection Radar Technique for Precipitation Mosaic Nowcasting”, IEEE journal of selected topics in applied earth observations and remote sensing, vol. 5, no. 3, pp. 874 884 June **2012**
- **Osrodka K.**, Szturc J. and Jurczyk A. “Chain of data quality algorithms for 3-D single polarization radar reflectivity (RADVOL-QC system)”, Meteorol. Appl., DOI: 10.1002/met.1323, **2012**
- **Park, S.**, Maki, M., Iwanami, K., Bringi, V. N., and Chandrasekar, V., “Correction of radar reflectivity and differential reflectivity for rain attenuation at X-band, Part II: Evaluation and application”, J. Atmos. Ocean. Technol., vol. 22, no. 11, pp. 1633–1655, Nov. **2005**
- **Rinollo, A.**, Vulpiani, G., Puca, S., Pagliara, P., Kaňák, J., Lábó, E., Okon, Ł., Roulin, E., Baguis, P., Cattani, E., Laviola, S. and Levizzani, V. “Definition and impact of a quality index for radar-based reference measurements in the H-SAF precipitation product validation” Nat. Hazards Earth Syst. Sci., 13, pp. 2695-2705, **2013**
- **Šálek, M.**, Cheze, J.-L., Handwerker, J., Delobbe, L. and Uijlenhoet, R. “Radar techniques for identifying precipitation type and estimating quantity of precipitation”, COST Action 717. Luxembourg, **2004**
- **Steiner, M.**, Houze, R. A. Jr and Yuter, S. E. “Climatological characterization of three-dimensional storm structure from operational radar and rain gauge data”, J. Appl. Meteorol. 34: 1978–2007, **1995**
- **Tabary, P.**, Le Henaff, G., Dupuy, P., Parent du Chatelet, J. and Testud, J. “Can we use polarimetric X-band radars for operational quantitative precipitation estimation in heavy rain regions?”, In Proceedings of Weather Radar and Hydrology International Symposium. -Grenoble, 10-15 March **2008**
- **Tabary, P.** “The new French operational radar rainfall product. Part I: methodology”, Weather Forecast., 22, 393– 408, **2007**
- **Villarini, G.** and Krajewski, W. F. “Review of the different sources of uncertainty in single polarization radar-based estimates of rainfall”, Surv. Geophys., 31 (1), 107– 129, **2010**
- **Zawadzki, I.** “Sense and nonsense in radar QPE”, *Proceedings of ERAD 2006: 4th European Conference on Radar in Meteorology and Hydrology*, pp. 121–124, ISBN 978- 84-8181-227-5, Barcelona, Spain, September 18-22, **2006**